Equilibrium behavior of sessile drops under surface tension, applied external fields, and material variations

Benjamin Shapiro[a]
Aerospace Engineering Department, University of Maryland at College Park, Maryland 20742

Hyejin Moon
Mechanical and Aerospace Engineering Department, University of California at Los Angeles (UCLA), Los Angeles, California 90095

Robin L. Garrell
Department of Chemistry and Biochemistry, University of California at Los Angeles (UCLA), Los Angeles, California 90095

Chang-Jin "CJ" Kim
Mechanical and Aerospace Engineering Department, University of California at Los Angeles (UCLA), Los Angeles, California 90095

This article describes the equilibrium shape of a liquid drop under applied fields such as gravity and electrical fields, taking into account material properties such as dielectric constants, resistivities, and surface tension coefficients. The analysis is based on an energy minimization framework. A rigorous and exact link is provided between the energy function corresponding to any given physical phenomena, and the resulting shape and size dependent force term in Young's equation. In particular, the framework shows that a physical effect, such as capacitive energy storage in the liquid, will lead to $1/R$ "line-tension"-type terms if and only if the energy of the effect is proportional to the radius of the liquid drop: $E \propto R$. The effect of applied electric fields on shape change is analyzed. It is shown that a dielectric solid and a perfectly conducting liquid are all that is needed to exactly recover the Young–Lippmann equation. A dielectric liquid on a conducting solid gives rise to line tension terms. Finally, a slightly resistive liquid on top of a dielectric, highly resistive solid gives rise to contact angle saturation and accurately matches the experimental data that we observe in our electro-wetting-on-dielectric devices. © *2003 American Institute of Physics.* [DOI: 10.1063/1.1563828]

I. INTRODUCTION

The shape of a liquid drop on a surface is determined by the composition of the liquid (solvent, and ionic and surfactant solutes) and by the composition and morphology of the underlying solid. When an electric potential is applied across the liquid drop and the solid substrate, ions and dipoles redistribute in the liquid, in the solid, or in both depending on the relative material properties. This redistribution can cause a hydrophobic surface to behave in a hydrophyllic manner. In such a case, the liquid drop will change shape under the applied electric potential.

This electro-wetting phenomenon can be used to create fluid flow. [1–10] In practice, electro-wetting-based actuation of aqueous solutions is limited by the onset of current flow through the substrate and the solution, which leads to chemical oxidation, the reduction of solutes, and to electrolysis (bubble formation). It has recently been demonstrated that fluid actuation can be achieved without electrolysis by coating the conductor or semiconductor substrate with a dielectric. [1,3,6,10] The dielectric serves both to block the elec-

tron transfer and to provide a hydrophobic surface that enables large changes in contact angle. This electro-wetting-on-dielectric (EWOD) driven actuation has been used to create droplets from reservoirs, as well as to cut, join, and mix drops on planar surfaces or in channels. [3,10] Applications of EWOD include microfluidics and biofluidic sensors and devices.

In order to design and control such devices, we required accurate models of the underlying physics. First, we need some way of deciding which physical mechanisms are dominant in the devices: is the ionic double-layer more or less important then the dielectric energy stored in the liquid? What percent of the energy is being stored/dissipated in the liquid bulk, solid bulk, and at the interfaces? Second, we need to understand the engineering limits: why does contact angle saturate? What limits droplet switching speed? This article addresses some of these needs.

A. Background

Prior modeling results are based on the classical work by Lippmann [11] and Young (see, for example, Chap. 10 in Probstein [12]). More recent articles include Refs. 1,7,10,13–25. In particular, the total energy minimization framework proposed by Digilov [26] is similar to our starting point. How-

---

[a]Author to whom correspondence should be addressed; electronic mail: benshap@eng.umd.edu; http://www.glue.umd.edu/~benshap/

ever, our method of analysis and physical interpretation is different; plus, we go on to numerically solve the surface-energy/electrostatic minimum energy conditions and we study the properties of the solutions.

Due to its engineering importance, there have been a large number of articles focused on electro-wetting limiting phenomena: why does the contact angle cease to change after some critical voltage is reached? To date, some of the proposed physical mechanisms include: electrolysis,[24] contact line electrostatic/capillary instabilities for pure water,[6] ionization of air in the vicinity of the drop edge,[6] charge trapping,[5] and a proposed zero surface/liquid energy limit.[4] Charge/ion adsorption from the liquid to the solid surface, and its effect on the solid/liquid surface energy, is another possible source of contact angle saturation. [27,28] The match between contact angle saturation theory and experiment is often inconclusive, and/or the model parameters have been chosen to fit one set of data but have not been validated against a different independent set of data. (A notable exception is the work of Verheijen and Prins. [5] These authors show good agreement between experiment and theory and they present a second independent test to show that charge trapping is responsible for contact angle saturation in their devices.) It is possible, in fact likely, that different limiting phenomena are important in different devices: Vallet, Vallade, and Berge [6] see luminescence in their devices and argue that gas ionization is one of their dominant phenomena. We do not see any luminescence in our devices but we have been able to accurately predict contact angle saturation for multiple devices, without fitting, by including the small electrical resistance found in the liquid.

There have also been a number of studies about the electrical and chemical details at the interfaces: Lyklema[29] presents a comprehensive discussion of ion double-layer theories; Chou[30] presents an analytic solution for the liquid/gas shape right at the triple point under an applied potential; Zimmerman, Dukhin, and Werner[31] provide an experimental and theoretical treatment of ζ potentials and solid/liquid conductivities due to ion adsorption; and Koopal and Avena[32] provide an excellent description of adsorption kinetics. We do not consider such fine-scale spatial details here.

B. Current approach

Our analysis is aimed at quantifying how different physical effects (gravity, electrical resistance, ionic double layers) influence the electro-wetting phenomena. In this article we are only interested in those physical phenomena that influence voltage induced shape change. Essentially, we need some way of deciding which physical effects are important and which are negligible. We do this by finding the energy associated with each effect, by minimizing the energy to find equilibrium conditions, and by rigorously converting that energy minimum into a Young-type equation that describes the change in droplet shape as a function of applied voltage and other physical parameters. This lets us compare the relative sizes of different effects. In this sense, our analysis is similar in spirit to Digilov.[26] However, when necessary, we phrase and solve Maxwell's partial differential equations to find the

electric fields, and thus the stored energies, inside the solid and liquid materials. Moreover, we have been able to derive a rigorous equation which takes any arbitrary energy term and analytically gives back the corresponding, size-dependent, force term in Young's equation.

Section II A presents the mathematical framework that takes the energy term for any physical effect and computes the resulting force term in Young's equation. Sections III A and III B verify this framework for two simple examples where the answer is known and is straightforward, respectively. New ground is covered in Secs. IV A 4 and IV B, culminating with the contact angle saturation example of Sec. IV C.

The basic tenets of our analysis are: a total energy minimization, a phrasing of Maxwell's electrostatic partial differential equations (PDEs), an analytical extraction of how the PDE solutions change with analytically accessible parameters, and a numerical solution of the remaining, normalized, shape-dependent PDEs to capture parametric dependences that are not available analytically.

a. *A total energy minimization approach with a constant liquid volume constraint*: We write down the energy due to liquid/gas, liquid/solid and solid/gas interfaces plus the energy stored in the bulk due to applied external fields such as gravity and the imposed electrical potentials. The energy is minimized subject to the constraint that the liquid volume must remain the same. This gives rise to a Young-type equation that can account for any physical effects and which includes droplet size dependence.

Although the link between energetics and Young-type formulations has been explored partially (see, for example, Chap. 10 in Probstein[12] and Refs. 16 and 15) this argument has traditionally been applied for a pure translation of the liquid/gas front: no change in droplet size is considered. This means that the radius R does not appear in the formulation, and so all the size information is lost. Using this approach, it is fundamentally impossible to recover size dependent terms like the "line-tension" $1/R$-type term debated in the literature. This term is usually included based on phenomenological considerations, not derived from first principles, hence the debate. Our analysis includes variations in both R and θ and analytically recovers the size dependent terms. Thus, given the energy due to any physical effect, we can analytically write down the corresponding force term in Young's equation. In particular, we can state when line tension terms exist, and we can derive these terms from physical first principles.

b. *Solution scalings for the electrostatic partial differential equations (PDEs)*: In order to find the electrical energies, we first find the PDEs and the relevant boundary conditions that describe the electric fields inside the liquid and solid phases. (Typically, Maxwell's equations are sufficient for phrasing the right set of PDEs. But there are cases where we consider other coupled effects such as the thermal diffusion effects found in the ionic double layer.) Before solving the resulting PDEs, we perform an analytic scaling analysis to extract as many parametric dependencies as possible. By so doing, we find how the solutions, and also the electrical energies, scale with system parameters such as the applied volt-

age V and liquid radius R, and with intrinsic material coefficients such as the resistivities ρ and dielectric constants ϵ. In most instances, this type of analysis is sufficient to reveal the underlying nondimensional numbers that determine the strength of the various physical phenomena. For example, the Bond number $B = \rho g R^2 / \gamma_{\mathrm{lg}}$ which determines the size of gravity terms compared to surface tension effects can be recovered from a scaling analysis.

c. *Solving the shape-dependent normalized PDEs*: Once we have extracted the dimensional parameters such as the voltages, radius, heights, dielectric constants and resistivities, it remains to solve the PDEs for the shape, or θ, dependence. This is done numerically.

d. *Finding the energy minima*: From the scaling analysis and the shape-dependent numerical results, we can find the total electrical energies as a function of the applied fields, material coefficients and droplet shape. By minimizing this energy, we can find the contact angle as a function of parameters. At the end, the result depends only on a few dimensionless numbers. In the case of gravity, the contact angle depends on the nondimensional surface tension number Γ and the Bond number B. In the case of a resistive liquid atop a dielectric solid, the contact angle depends on the surface tension coefficient Γ, on the insulating solid electro-wetting number U, and on the nominal ratio of solid to liquid resistance $\bar{A}_o$.

e. *Predict key phenomena, including line-tension and contact angle saturation*: This article essentially performs a careful engineering analysis of the bulk electrical and surface tension properties of a sessile drop. Using this approach we have been able to rigorously show that a dielectric liquid leads to $1/R$ line tension terms, but a conducting liquid does not. We have been able to assess the electrical resistive-capacitive (RC) charging time constants, and we have been able to quantitatively predict contact angle saturation in our devices. It will be shown that saturation, at least in our devices, is caused by the small amount of electrical resistance found in the liquid. This explains why we continue to see essentially the same contact angle saturation behavior for different dielectric coatings of different thicknesses: the saturation is basically fixed by the net resistance of the liquid which depends on its size R, shape θ, and its intrinsic resistivity ρ_l.

II. ASSUMPTIONS AND THE MATHEMATICAL FRAMEWORK

Our attention is restricted to a single, approximately spherical, sessile drop in equilibrium, under applied external fields (such as gravity and electric potentials), with variable material properties (solvent, ion type and concentration, and the dielectric constants of the liquid and solid). For this case, the modeling framework and underlying assumptions are listed below.

a. *An energy minimization approach*: We phrase all physical effects in terms of energies (not forces). From a tautological standpoint this is attractive because all known forces are derivatives of a potential energy (see Vol. I, Chap. 14, Sec. 4 in Feynman[33]). Nonconservative forces, which are
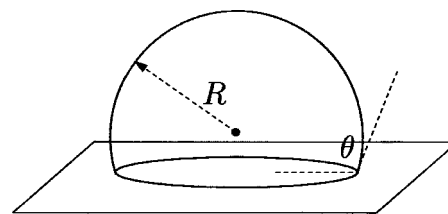

FIG. 1. Spherical drop geometry is parametrized by radius R and (apparent) contact angle θ.

not written as the derivatives of a potential energy, are used when it is not possible to track the details of all the underlying conservative forces. An energetics framework is also advantageous from a practical standpoint. It is not at all clear how ion diffusion gradients give rise to forces at the triple-phase line, but it is (relatively) straightforward to find the potential energy associated with an ion distribution field, and to then perform the energy differentiation described in Sec. III to find the associated term in Young's equation.

b. *Drop shape*: The drop is assumed to be essentially a perfect sphere truncated at the solid plane, as shown in Fig. 1. High gravitational or electrical forces can squash a drop but we assume that the applied external fields are sufficiently small that this distortion is negligible. We also neglect any droplet deformation right at the triple line because we are only interested in the bulk, not local, shape of the drop. This means that the shape of our drop can be uniquely described by two numbers: the radius R and the contact angle θ. After we have solved for the electric, gravitational, and other fields as a function of R and θ, the liquid drop has only these two degrees of freedom left. The constant liquid volume constraint ties R and θ together and thus reduces the problem to a single degree of freedom.

The methods in this article can be extended to nonspherical drops and puddles. In such cases, the spirit of the development is exactly the same, but the associated mathematics needed to find the larger number of parameters to describe the minimal energy liquid shape is more sophisticated. See Brakke[34] for how to compute complex minimal energy surfaces.

c. *Equilibrium*: Thus far we have only addressed the equilibrium shape of the liquid drop under applied fields and material variations. To include droplet dynamics, which are important for issues such as maximizing droplet switching speed in the electro-wetting devices described in Cho *et al.*,[35] two extensions will be required.

First, we will have to consider the time varying nature of the electric fields. This is done partially in Secs. IV C 1 and IV C 2 where we find that our resistive-capacitive (RC) charging time constants are on the order of milliseconds. Second, and more importantly, it will be necessary to incorporate our results into fluid simulations that solve the low-Reynolds limit of the Navier-Stokes equations for two-phase flows. Two points are important. A common concern is the validity of the continuum assumption (see Beskok[36] for a good overview) which is not an issue in our micrometer sized devices. Also, there is an inconsistency between surface tension contact angle and viscous no-slip fluid boundary

conditions:[15,17,19,37] if both boundary conditions are enforced, and if the fluid is a realistic fluid where discontinuous velocity fields are not possible, then the triple line cannot move. Resolution of this issue is an active area of research.

d. *No roughness or hysteresis*: No surface roughness effects are included in the current model. The contact angle hysteresis that arises from surface heterogeneities or roughness can be modeled by energy considerations,[21] and thus can be incorporated into the current framework.

e. *No evaporation*: The liquid volume of the droplet shown in Fig. 1 is assumed to remain constant. If we wanted to include the liquid volume change associated with evaporation, we would need to formulate the energies associated with phase change and let volume become a variable instead of a fixed parameter.

Rigorous conversion from energy minimum to the modified Young's equation

This section presents the mathematics for converting any sessile drop potential energy function (including energies for effects such as ion concentrations, electric fields, and material variations) into a Young-type equation. This link is rigorous and exact: there are no approximations associated with the conversion. All approximations reside within incomplete knowledge of the energies, or within the assumption that the drop is a perfect sphere completely described by radius R and contact angle θ. In Sec. III we will find the total potential energy $E(R,\theta;p)$ of the drop for different physical scenarios. At the end of all computations, this energy will depend on the drop radius R, the (apparent) contact angle θ, and relevant system parameters p such as applied voltage V, dielectric constants ϵ_ℓ and ϵ_s, and nominal liquid ion concentrations c_o.

At equilibrium, the drop will assume a shape R,θ that minimizes this energy E. This means that the derivative of the energy with respect to R and θ is zero

$$dE = \left[\frac{\partial E}{\partial R}(R,\theta;p)\right]dR + \left[\frac{\partial E}{\partial \theta}(R,\theta;p)\right]d\theta = 0. \qquad (1)$$

Equation (1) says that at an energy minimum, the infinitesimal change in energy due to shape variations must be zero, and that there are two possible shape variations: one in R and the other in θ. It is not possible to change θ without also changing R; if θ increases in Fig. 1, R must decrease to keep the drop volume constant (neglecting evaporation). The drop volume is given by

$$v(R,\theta) = \pi R^3 \left(\frac{2}{3} - \frac{3\cos\theta}{4} + \frac{\cos 3\theta}{12}\right). \qquad (2)$$

Since volume is constant, its variation must be zero, hence

$$dv = \left[\frac{\partial v}{\partial R}(R,\theta)\right]dR + \left[\frac{\partial v}{\partial \theta}(R,\theta)\right]d\theta$$

$$= \left[3\pi R^2 \left(\frac{2}{3} - \frac{3\cos\theta}{4} + \frac{\cos 3\theta}{12}\right)\right]dR$$

$$+ \left[\pi R^3 \left(\frac{3\sin\theta}{4} - \frac{\sin 3\theta}{4}\right)\right]d\theta = 0. \qquad (3)$$

Solving for dR in terms of $d\theta$ yields

$$dR = Rq(\theta)d\theta = R\left(-\frac{2\cos^2(\theta/2)\cot(\theta/2)}{2+\cos\theta}\right)d\theta, \qquad (4)$$

where $q(\theta) = -[2\cos^2(\theta/2)\cot(\theta/2)]/[2+\cos\theta]$. A similar equation is derived in Decamps and De Coninck.[20] Using Eq. (4), Eq. (1) can now be rewritten to show how the energy changes with contact angle

$$\frac{dE}{d\theta} = \left[\frac{\partial E}{\partial R}(R,\theta;p)\right]Rq(\theta) + \left[\frac{\partial E}{\partial \theta}(R,\theta;p)\right] = 0. \qquad (5)$$

In order to get the traditional Young term $\gamma_{lg}\cos\theta$ to appear in this equation, it is necessary to pre-multiply Eq. (5) by $-(2+\cos\theta)/2\pi R^2\sin\theta$. This term is strictly negative for all possible contact angles $0 < \theta < \pi$ so there is no division by zero. Thus

$$\left(-\frac{2+\cos\theta}{2\pi R^2\sin\theta}\right)\frac{dE}{d\theta}$$

$$= \left(-\frac{2+\cos\theta}{2\pi R^2\sin\theta}\right)\left(\left[\frac{\partial E}{\partial R}(R,\theta;p)\right]Rq(\theta)\right.$$

$$\left. + \left[\frac{\partial E}{\partial \theta}(R,\theta;p)\right]\right) = 0 \qquad (6)$$

is exactly Young's equation, although written in a new way.

In the special case when E only includes the energies due to liquid/solid, liquid/gas, and solid/gas interfaces with constant surface tension coefficients, as in Sec. III A, this equation becomes exactly $\gamma_{lg}\cos\theta - (\gamma_{gs} - \gamma_{ls}) = 0$. However, this formulation can handle any potential energy function $E(R,\theta;p)$. If we include additional effects such as electrical energy in the solid, electrical energy in the liquid, gravitational terms, or ion concentration effects, then Eq. (6) will rigorously produce additional terms in Young's equation.

III. TWO EXAMPLES AND THE SIZE DEPENDENT TERMS

The first example is a drop that only has energies due to interfaces. The purpose of this example is to verify the framework of Sec. II A and to show that we exactly recover the traditional Young equation in this simple case. The second example includes gravity. This example shows how bulk effects are included in the analysis, the electrical fields of Sec. IV are included in the same way, and it demonstrates how scaling arguments can be used to extract the relevant nondimensional parameters. We close this section with subsection III C which converts size dependent energy terms into the corresponding size dependent terms in Young's equation. This subsection shows when $1/R$ line-tension terms are active.

A. Interfacial potential energy

We start with a trivial example. If we only consider the potential energy due to the solid/liquid, solid/gas, and liquid/gas interfaces, and if we assume the surface tension coefficients are constant, then the sessile drop interfacial potential energy is given by Probstein[12] in Chap. 10

$$E_{\text{int}} = (\gamma_{\text{ls}} - \gamma_{\text{gs}})A_{\text{ls}} + \gamma_{\text{lg}}A_{\text{lg}}, \tag{7}$$

where the subscripts l, s and g denote liquid, solid, and gas phases, respectively, A_{ij} is the interface area (so A_{lg} is the area of the liquid/gas interface), and γ_{ij} are the surface tension coefficients with units of energy per area. The solid/gas coefficient γ_{gs} appears with a negative sign because if A_{ls} is increased by some amount, then A_{gs} must be decreased by the same amount.

For the drop shown in Fig. 1, it follows from purely geometrical reasoning that

$$A_{\text{ls}}(R, \theta) = \pi R^2 \sin^2 \theta, \tag{8}$$

$$A_{\text{lg}}(R, \theta) = 2\pi R^2 (1 - \cos \theta). \tag{9}$$

In consequence, the interfacial potential energy is

$$E_{\text{int}}(R, \theta) = R^2 [(\gamma_{\text{ls}} - \gamma_{\text{gs}})\pi \sin^2 \theta + \gamma_{\text{lg}} 2\pi (1 - \cos \theta)]. \tag{10}$$

As expected, the interfacial potential energy term scales with drop radius squared. If we plug E_{int} into the conversion described by Eq. (15), then, after some half angle trigonometric identities, we exactly recover the traditional Young equation[12] $\gamma_{\text{lg}} \cos \theta - (\gamma_{\text{gs}} - \gamma_{\text{ls}}) = 0$.

B. Gravitational potential energy

We now consider the potential energy due to gravity. This case is presented because it demonstrates some of the key concepts, such as solution scaling, for a simple and intuitive example. In reality, for most practical microfluidic devices, gravity is negligible.

It is possible to find the form of the gravitational potential by a simple scaling analysis.

A liquid element of volume Δv, of density ϱ, at height ℓ above the solid reference plane, will have a potential energy due to gravity of $\Delta E_{\text{gvty}} = mg\ell = \varrho g \ell \Delta v$, where $m = \varrho \Delta v$ is the mass of the element and $g = 9.81 \, \text{m/s}^2$ is the acceleration due to gravity. The total potential energy due to gravity is the integral over all the liquid elements within the drop shape. For a drop of radius one, the integral of $\varrho g \ell \, dv$ over the drop shape will give some function of θ only: $E_{\text{gvty}}(R = 1, \theta) = a_{\text{gvty}}(\theta)$. If we increase the size of the drop by a factor of R but keep the shape, meaning θ, the same, then the integral will change by a factor of R^4 – the "number" of elements remains the same, but there is one factor of R for the change in ℓ and three factors of R for the cubic change in dv. Hence the potential energy of the drop due to gravity must be

$$E_{\text{gvty}}(R, \theta) = R^4 a_{\text{gvty}}(\theta), \tag{11}$$

where $a_{\text{gvty}}(\theta)$ is the shape form factor. This R^4 dependence will create an R^2 term in Young's equation: $\gamma_{\text{lg}} \cos \theta = (\gamma_{\text{gs}} - \gamma_{\text{ls}}) + R^2 b(\theta)$, as described by Eq. (15) in Sec. III C below.

To actually find the form factor a_{gvty}, we carry out the shape integration. Namely

$$a_{\text{gvty}}(\theta) = \int_{\pi - \theta}^{\pi} -\pi \varrho g [\cos \phi + \cos \theta] \sin^3(\phi) \, d\phi$$

$$= \frac{2\pi}{3} \varrho g [3 + \cos \theta] \sin^6(\theta/2). \tag{12}$$

As necessary, this factor is zero when $\theta = 0$ (total spreading corresponds to an infinitely thin, infinitely large puddle and means no potential energy due to gravity) is maximal when $\theta = \pi$ (no wetting), and is strictly positive for all θ in between.

Combining this result with the Eqs. (10) and (11), the potential energy due to the interfacial and gravitational terms is

$$E(R, \theta) = R^2 [(\gamma_{\text{ls}} - \gamma_{\text{gs}})\pi \sin^2 \theta + \gamma_{\text{lg}} 2\pi (1 - \cos \theta)]$$

$$+ R^4 \varrho g \frac{2\pi}{3} [3 + \cos \theta] \sin^6(\theta/2). \tag{13}$$

The interfacial term is at a minimum when θ is equal to the no gravity equilibrium contact angle. The gravity term is at a minimum when $\theta = 0$ and so it tends to flatten the drop: its effect is more pronounced for larger drops where the Bond ratio $B = R^4 \varrho g / R^2 \gamma = R^2 \varrho g / \gamma$ is substantial. A standard calculation shows that for a 0.1 mm sized drop of water, the Bond number is approximately $(10^{-4} \, \text{m})^2 \times (10^3 \, \text{kg/m}^3) \times (9.81 \, \text{m/s}^2)/(\gamma_{\text{lg}} = 7.3 \times 10^{-2} \, \text{kg/s}^2) = 0.0013$, which means that the gravity potential energy is only 0.1% of the interfacial energy.

Using Eq. (15) derived below, and dividing through by γ_{lg}, the dimensionless Young's equation for a liquid drop with gravity is

$$\cos \theta - \left(\frac{\gamma_{\text{gs}} - \gamma_{\text{ls}}}{\gamma_{\text{lg}}}\right) + \left(\frac{R^2 \varrho g}{\gamma_{\text{lg}}}\right)\left[\frac{\cos \theta}{3} - \frac{\cos 2\theta}{12} - \frac{1}{4}\right] = 0. \tag{14}$$

C. $R^k a(\theta)$ energy terms lead to $R^{k-2} b(\theta)$ Young terms

As shown in the two examples above, many potential energy terms scale as $E(R, \theta) = R^k a_k(\theta)$ where R^k is the size dependence and a_k is a shape factor. Interfacial energy terms in Sec. III A scale as $R^2 a_2(\theta)$, gravity terms scale as $R^4 a_4(\theta)$ in Sec. III B, the conducting drop will have a $R^2 a_2(\theta)$ scaling (Sec. IV A), and the dielectric drop will display a $R a_1(\theta)$ scaling (Sec. IV B). Some physical effects, like the fixed electrode height resistivity effect of Sec. IV C 4, will lead to energies that do not scale simply as powers of R. But even in this case we can expand such terms into a power series in R, or we can just apply Eq. (6) directly without the additional analysis described below.

Using Eq. (6), we see that a $E = R^k a_k(\theta)$ energy term gives a

Young's equation term for a $E_k = R^k a_k(\theta)$ energy term

$$
\begin{aligned}
&= \left(-\frac{2+\cos\theta}{2\pi R^2 \sin\theta} \right) \left(\frac{\partial E}{\partial R} Rq(\theta) + \frac{\partial E}{\partial \theta} \right) \\
&= \left(-\frac{2+\cos\theta}{2\pi R^2 \sin\theta} \right) \left(kR^{k-1}a_k(\theta)Rq(\theta) + R^k \frac{\partial a_k}{\partial \theta} \right) \\
&= R^{k-2} \left(-\frac{2+\cos\theta}{2\pi \sin\theta} \right) \left(ka_k(\theta)q(\theta) + \frac{\partial a_k}{\partial \theta}(\theta) \right) \\
&= R^{k-2}b_k(\theta) \qquad\qquad\qquad\qquad\qquad\qquad (15)
\end{aligned}
$$

contribution in Young's equation. R^4 energy terms (e.g., gravity) lead to R^2 effects in Young's equation, $R^2 a_2(\theta)$ energy terms (e.g., interfacial areas or insulating dielectric solids) reduce to pure θ terms, and $Ra_1(\theta)$ terms lead to $1/R$ line-tension variations. This means that the conducting liquid drop in Sec. IV A whose electrical energy scales as R^2 will produce a Young's equation with no R dependence. However, the dielectric liquid drop whose energy scales as $Ra(\theta)$ will have a line tension term, and the magnitude of this term will be determined by the energy derivation in Sec. IV B and by Eq. (15).

IV. THREE EXAMPLES WITH ELECTRICAL ENERGIES

Here we consider three examples that include electrical fields. A conducting liquid atop a dielectric solid is discussed in Sec. IV A: this recovers the traditional Lippmann–Young relation. In this section we also address the role of the ionic double layer. A dielectric liquid atop a conducting solid is analyzed in Sec. IV B: this case leads to a $1/R$ line tension term. Section IV C considers a slightly resistive liquid atop a highly resistive dielectric solid this case recovers the contact angle saturation behavior we observe in our devices. For each example, we find the total potential energy, extract the nondimensional parameters, and find the dimensionless, modified Young's equation.

A. Conducting liquid atop a dielectric solid

In bio-chip applications, the water will contain an appreciable number of ions and will be a good conductor of electricity: see Probstein,[12] Sec. 2.5, for a relation between ion concentrations and the resistivity or conductivity of water. To prevent current flow, the dielectric coatings in our EWOD devices[35] are designed to act as insulators. Thus, to a first approximation, the experimental arrangement in EWOD devices can be described as a conductive liquid above an insulating, dielectric solid. It will be shown that this conducting liquid/ insulating solid case exactly recovers the Lippmann–Young relation $\gamma_{lg}\cos\theta = [\gamma_{gs} - \gamma_{ls} + \epsilon_s V^2/2h]$, but it does not lead to contact angle saturation or any line tension $1/R$-type terms.

Figure 2 shows the relevant geometry. Because the liquid is conductive, the potential at the solid/liquid interface is equal to the applied voltage: $\phi_{sl} = V$. There are three sources of potential energy: the interfacial energy derived in Sec. III A, the dielectric energy stored in the solid, and the energy stored in the externally applied charging source.
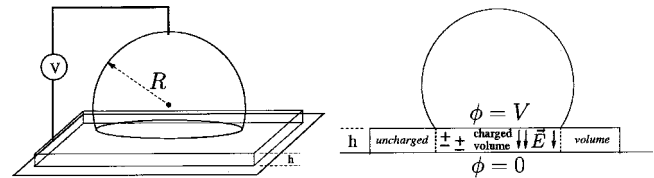

FIG. 2. Left: Conducting drop atop an insulating dielectric layer of thickness h. The voltage V is applied between the bottom-most flat conducting electrode and the electrode inserted into the top of the drop. Right: Schematic showing resulting dipole moments $\pm$ in the dielectric immediately under the liquid/solid contact area; here the electric field $\mathbf{E} = -(0,0,V/h)$ points down as shown by the arrows. The electric field is zero everywhere else.

1. Potential energy in the solid dielectric layer

For a dielectric solid element at location (x,y,z), of volume Δv, with local electric field $\mathbf{E}(x,y,z)$; the electrical potential energy is $\Delta E_{de} = \frac{1}{2}(\mathbf{D}\cdot\mathbf{E})\Delta v$. Here $\mathbf{D}$ is the polarazibility vector field: it is the induced dipole moment in the solid per unit volume, see Feynman[33] Volume II, Chap. 10, Sec. 2. For an ideal dielectric, this moment is linearly related to the local electric field by $\mathbf{D} = \epsilon_s \mathbf{E}$ where ϵ_s is the dielectric constant of the sold. Hence $\Delta E_{de} = \frac{1}{2}\epsilon_s|\mathbf{E}|^2\Delta v$. Neglecting edge effects, the electric field immediately under the solid/liquid contact area is $\mathbf{E} = -(0,0,V/h)$; it points straight down with a strength equal to the applied voltage V divided by the dielectric thickness h. The electric field everywhere else is zero as illustrated in Fig. 2. Thus $\frac{1}{2}\epsilon_s|\mathbf{E}|^2 dv$ must be integrated over the volume $v = hA_{ls}$ and this gives, together with Eq. (8), the energy stored in the solid dielectric

$$
E_{de}(R,\theta) = \frac{1}{2}\epsilon_s \left(\frac{V}{h}\right)^2 hA_{ls} = \frac{\epsilon_s V^2}{2h}\pi R^2 \sin^2\theta. \qquad (16)
$$

If there are n solid dielectric layers, as opposed to the single dielectric layer considered above, then ϵ_s/h is replaced by the net in-series capacitance per unit area $1/(h_1/\epsilon_1 + \ldots + h_n/\epsilon_n)$.

2. Potential energy stored in the external charging source

The basic reason this term has to be included is that every time the drop shape changes, the charged volume immediately under the solid/liquid contact area changes, and a packet of charge ΔQ must be received from or pushed back against the fixed voltage source. This requires an amount of work, or minus potential energy, $W = V\Delta Q = -E$. It follows that the energy stored in the charge source is twice again the energy stored in the dielectric but with opposite sign. A careful exposition of this result can be found in Vol. II, Chap. 8, Sec. 2 of Feynman[33] and also in Verheijen and Prins,[5] and so it is not repeated. Hence $E_{cs}(R,\theta) = -(\epsilon_s V^2/h)\pi R^2 \sin^2\theta$.

3. Total energy and the Young–Lippmann equation

Combining the interfacial energy of Sec. III A with the dielectric and external source energy derived above, the total energy for the conducting drop system is

$$E(R,\theta)=R^2\left[\left(\gamma_{\mathrm{ls}}-\gamma_{\mathrm{gs}}-\frac{\epsilon_s V^2}{2h}\right)\pi\sin^2\theta+\gamma_{\mathrm{lg}}2\pi(1-\cos\theta)\right].$$

(17)

Note that ϵ_s is the dielectric constant of the solid, not the liquid.

Equation (17) is identical to Eq. (10) except that $\gamma_{\mathrm{ls}}-\gamma_{\mathrm{gs}}$ has become $\gamma_{\mathrm{ls}}-\gamma_{\mathrm{gs}}-\epsilon_s V^2/2h$. Using the results of Eq. (15), and dividing through by γ_{lg} to nondimensionalize, we exactly recover the Lippmann–Young relation

$$\cos\theta-\left(\frac{\gamma_{\mathrm{gs}}-\gamma_{\mathrm{ls}}}{\gamma_{\mathrm{lg}}}+\frac{\epsilon_s V^2}{2\gamma_{\mathrm{lg}}h}\right)=0.$$

(18)

This equation contains no line tension $1/R$ terms because the energy stored in the dielectric scales as the charged volume in the solid, and this volume scales as $A_{\mathrm{ls}}h\sim R^2h$. Since h is constant, this stored energy behaves just like a liquid/solid interfacial energy term. To get a line tension term, it is necessary to have a physical effect whose energy scales as R, not as R^2 (see Sec. IV B).

4. Effect of ionic double layer

There are two basic physical effects associated with the double layer. The first is the capacitive energy stored in the double layer: this effect is negligible in our devices. Lippmann theory treats the ionic double layer as a Helmholtz capacitor. As pointed out in Ref. 24, this is equivalent to treating the ionic layer as yet another material layer (so in our case we would then have three layers: silicon dioxide, Teflon, and the ionic layer). Since the thickness of the ionic layer (nm's) is much smaller than the thickness of the material coatings ($\mu m's$), the dielectric energy stored in the ionic double layer is negligible. It is possible to make this argument precise even when nonlinear effects in the ionic double layer are considered. For the standard fully dissociated, symmetric salt situation discussed in Refs. 38 and 12, it can be shown (see the Appendix) that the ratio of the energy stored in the double layer to the energy stored in the solid dielectric must fall below $\epsilon_s\lambda_D/\epsilon_l h_s$ which is on the order of 0.001 for our devices. Here ϵ denotes the dielectric constant in the liquid and solid, λ_D is the Deybe double layer length scale which is typically on the order of nanometers, while h_s is the height of the insulating solid layer and it ranges between 0.1 and 10 μm in our devices.

The second physical effect is the possible change in the liquid/solid surface tension coefficient γ_{ls} due to voltage induced surface chemistry. This effect can be important. In our devices, protein adsorption/desorption to the Teflon surface is modified by the applied voltage, and the adsorbed proteins change the surface tension properties of the Teflon appreciably.

Consider first a simpler case. For a standard fully dissociated symmetric salt, the change in the positive and negative ion concentration $\Delta c_{\pm}$ at the solid/liquid interface depends exponentially on the applied voltage as

$$\Delta c_{\pm}=c_o e^{\mp(zF/RT)V_{\mathrm{dl}}}$$

(19)

where c_o is the far field ion concentration, V_{dl} is the voltage drop across the double layer, and zF/RT is the characteristic
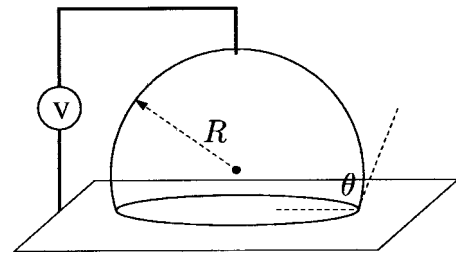

FIG. 3. A dielectric liquid drop with dielectric constant ϵ_l atop a conducting solid. The bottom plate has a zero ground potential $\phi=0$, but the liquid immediately surrounding the tip of the electrode at the top of the drop has a $\phi=V$ potential.

potential.[12,38] If, in turn, the solid/liquid surface tension coefficient γ_{ls} depends on the wall ion concentration, $\gamma_{\mathrm{ls}}=\gamma_{\mathrm{ls}}(c_{\pm})$, as stated in Butkus and Grasso,[28] then γ_{sl} becomes a function of the applied voltage. If $\gamma_{\mathrm{ls}}(c_{\pm})$ is known experimentally, say from Butkus and Grasso,[28] then Eq. (19) together with a voltage balance gives $\gamma_{\mathrm{ls}}=\gamma_{\mathrm{ls}}(V)$. This must then be substituted into Eq. (7) and the voltage dependent $\gamma_{\mathrm{ls}}(V)$ will then appear in Eq. (17) also. The methods of Sec. II A and Eq. (6) will now return the modified Young's equation for this case.

More complex situations, such as those involving protein adsorption/desorption, raise two key issues. First, how strongly does the liquid/solid surface tension coefficient γ_{sl} depend on the species concentration at the wall? Butkus and Grasso[28] find a moderate change in γ_{sl} based on electrolyte concentration. Van der Vegt *et al.*[27] find a much stronger variation of both the solid/liquid and liquid/gas surface tension coefficients. Second, what is the transport rate of the chemical species from the liquid bulk to the solid/liquid and liquid/gas interfaces? And how does this transport vary with applied voltage? As noted in van der Vegt *et al.*,[27] chemical species transport is a complex and important issue.

B. Dielectric liquid atop a conducting solid

We now compute the electric potential energy for a dielectric liquid drop with an applied voltage. This case is treated because we are interested in transporting dielectric liquids such as silicone oil, and because this case recovers the controversial $1/R$ line tension terms from physical first principles. Such terms are included in Refs. 26 and 22 based on phenomenological grounds. Below it is assumed that the drop is an insulator with dielectric constant ϵ_l and that the solid is a perfect conductor; for example, a droplet of silicone oil atop a metal electrode. A voltage V is applied as shown in Fig. 3.

1. Electrical energy scaling

For this case, we assume the top electrode is always positioned so that it only penetrates the tip of the drop. The analysis for a fixed electrode case is analogous to the analysis carried out in Sec. IV C 3. The end result for the fixed electrode case is similar to the varying electrode height case discussed here. Like in the gravity example, it is possible to find the form of the electrical potential energy by a scaling argument. As in Sec. IV A, the potential energy stored in a

small volume Δv of (ideal) dielectric material is $\Delta E_{de} = \frac{1}{2}\epsilon_l |\mathbf{E}|^2 \Delta v$, where ϵ_l is the dielectric constant of the liquid and $\mathbf{E}(x,y,z)$ is the electric field in the liquid.

To see how the electrical energy scales with voltage, radius, and the dielectric constant, we need to understand how the electric field $\mathbf{E}$ varies with these parameters. First consider a drop of unit radius with a unit applied voltage. The electric potential field within such a drop is described by Poisson's equation $\nabla^2 \phi(x,y,z) = 0$, with boundary conditions $\phi_{\text{bottom}} = 0$ and $\phi_{\text{top}} = V = 1$. (Side boundary conditions, which are independent of R and V, do not affect the scaling argument.) The electric field is then the gradient of the potential field: $\mathbf{E} = -\nabla\phi = -(\partial\phi/\partial x, \partial\phi/\partial y, \partial\phi/\partial z)$.

Consider the potential field $\phi(x,y,z)$ inside a drop of unit radius with applied unit voltage. If we double the size of the liquid drop then the potential field ϕ is stretched by a factor of 2: $\phi_{R=1}(x,y,z)$ becomes $\phi_{R=2}(x,y,z) = \phi_{R=1}(x/2,y/2,z/2)$. This means that the electric field, which is the rate of change of the potential in space, will become half as strong. Thus $\mathbf{E}_R(x,y,z) = 1/R \mathbf{E}_{R=1}(x/R,y/R,z/R)$. Conversely, if we double the applied voltage V then the electric field will be doubled. Therefore, if we know the electric field at position (x,y,z) for a drop of unit size with unit voltage, then the electric field at (Rx,Ry,Rz) for a drop of radius R with applied voltage V is

$$\mathbf{E}_{R,V}(Rx,Ry,Rz) = \frac{V}{R}\mathbf{E}_{R=1,V=1}(x,y,z). \qquad (20)$$

To find the stored potential energy, we must integrate the energy per unit volume $\Delta E_{de} = \frac{1}{2}\epsilon_l |\mathbf{E}|^2 \Delta v$ over the drop shape. Namely

$$E_{de} = \frac{1}{2}\int_{R,V \text{ drop}} \epsilon_l |\mathbf{E}_{R,V}|^2 dv,$$

$$= \frac{1}{2}\int_{R,V \text{ drop}} \epsilon_l \frac{V^2}{R^2} |\mathbf{E}_{R=1,V=1}|^2 dv,$$

$$= \frac{1}{2}\epsilon_l \frac{V^2}{R^2} R^3 \int_{R=1,V=1 \text{ drop}} |\mathbf{E}_{R=1,V=1}|^2 dv,$$

where the last equation is a consequence of the fact that the volume v scales as R^3. The integral in the last line only depends on the shape θ (both R and V are fixed to unity) hence

$$E_{de}(R,\theta) = \frac{1}{2}\epsilon_l R V^2 \int_{R=1,V=1 \text{ drop}} |\mathbf{E}_{R=1,V=1}|^2 dv$$

$$= \frac{1}{2}\epsilon_l R V^2 a_{de}(\theta). \qquad (21)$$

In summary, the electric field $\mathbf{E}$ varies as V/R; it appears twice in the potential energy giving a V^2/R^2 dependence, while the volume v scales as R^3. Together, they imply that the stored electrical energy for a dielectric liquid drop scales as $\frac{1}{2}\epsilon_l R V^2 a_{de}(\theta)$.
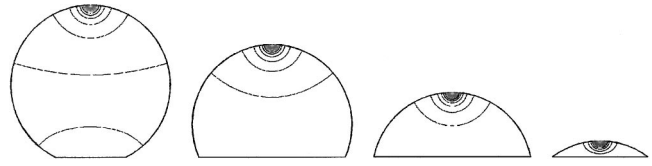

FIG. 4. Four drops of equal radius but different contact angles $\theta = 154°$, $114°$, $78°$, and $37°$. The constant electric potential contours $\phi(x,y,z) = c$ are shown for a vertical slice through each of the four drops. The calculated form factor for each drop is $a_{de}(\theta) = \int_{R=1,V=1 \text{ drop}} |\nabla\phi|^2 dv = 0.0592$, 0.0609, 0.0617, and 0.0640, respectively.

As in Sec. IV A, the potential energy stored in the voltage source is twice again the capacitive energy stored in the dielectric, but with opposite sign. Hence the total electrical energy stored in the system is

$$E_{\text{elec}}(R,\theta) = \frac{1}{2}\epsilon_l R V^2 a_{de}(\theta) - \epsilon_l R V^2 a_{de}(\theta)$$

$$= -\frac{1}{2}\epsilon_l R V^2 a_{de}(\theta). \qquad (22)$$

Equation (15) implies that the R dependence inside this term will give rise to a line-tension-type effect in Young's equation:

$$\gamma_{\text{lg}} \cos\theta = (\gamma_{\text{gs}} - \gamma_{\text{ls}}) + \frac{1}{R}b(\theta).$$

Thus we have been able to derive the phenomenological line tension term cited in Refs. 22 and 26 from physical first principles by using Sec. II A and a scaling argument.

2. Shape factor $a_{\text{de}}(\theta)$

To find the form factor $a_{de}(\theta)$, we need to solve Poisson's equation for all possible drop shapes. Figure 4 shows the electric potential field $\phi(x,y,z) = c$ contours for contact angles $\theta = 154°$, $114°$, $78°$, and $37°$.

Form factor results for 14 contact angles are shown in Fig. 5. Notice that $a_{de}(\theta)$ is nearly independent of θ for contact angles between $50°$ and $140°$. This is because all the high electric potential gradients $\nabla\phi$ that make up the majority of the integral occur at the top of the drop, or at the top and bottom when the contact angle is close to $180°$. Hence only a very small angle can impact the high gradient region at the top, and only a very large angle can create and then affect the high gradient region at the bottom.

Using the form factor of Fig. 5, together with Eq. (22), the potential energy for the interfacial plus electrical energy is

$$E(R,\theta) = R^2[(\gamma_{\text{ls}} - \gamma_{\text{gs}})\pi \sin^2\theta + \gamma_{\text{lg}} 2\pi(1-\cos\theta)]$$

$$-R\frac{\epsilon_l V^2}{2}a_{de}(\theta). \qquad (23)$$

Define $W = \epsilon_l V^2 / R \gamma_{\text{lg}}$ as the nondimensional dielectric liquid electro-wetting number. It is exactly this number that determines the size of the $1/R$ line-tension term. For a $R = 0.1$ mm drop of silicone oil with a dielectric constant of $\epsilon_l = 2.5\epsilon$ (from CRC handbook[39]) where ϵ is the permittivity
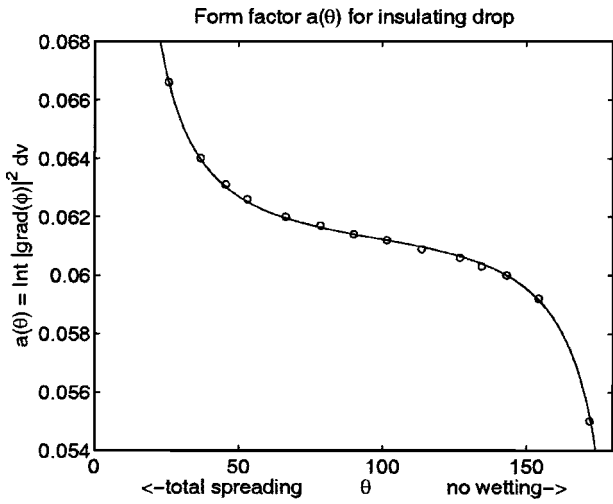
FIG. 5. Circles show the computed form factor $a_{de}(\theta)$ for 14 different contact angles. The stored energy in the liquid dielectric, for a drop of radius R with applied voltage V, is now given by $E_{de} = \frac{1}{2}\epsilon_l R V^2 a_{de}(\theta)$. Since the energy stored in a capacitor is $E_{de} = \frac{1}{2}CV^2$ this also gives the liquid drop capacitance as $C(\theta) = \epsilon_l R a_{de}(\theta)$. *Using θ in radians*, the equation for the solid line fit is $a_{de}(\theta) \approx 0.0592 + 0.0012\theta + 0.0022 \tan(1.71 - \theta)$ and it only holds for $0.4 < \theta < 3$ in radians, or equivalently for $25° < \theta < 172°$ in degrees.
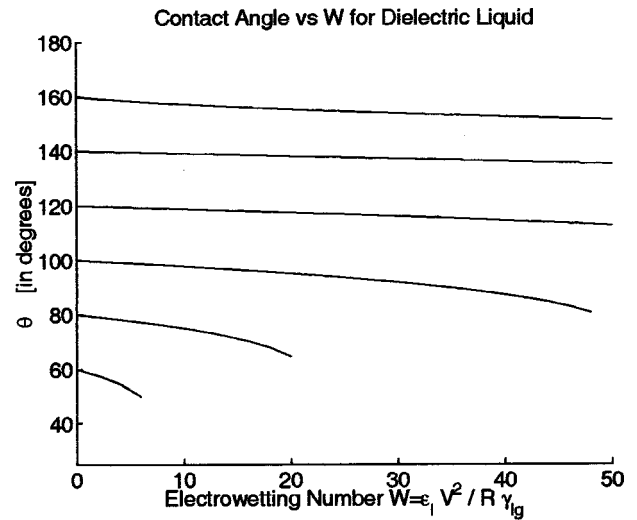

FIG. 6. For a dielectric liquid atop a conducting solid, this plot shows the contact angle dependence on the electro-wetting number $W = \epsilon_l V^2 / R \gamma_{lg}$ for six nominal (zero voltage) contact angles. The analysis above predicts that the drop shape will snap-to complete wetting past some critical electro-wetting number W^*. The predicted snap-to limit W^* is within the plot range for the three bottom curves. Three cautions are necessary: first, the shown snap-to situation for the bottom three curves corresponds to a very high electric field (the drop is thin and the voltage V is high); second, the fit for $a_{de}(\theta)$ used to generate these results does not hold for $\theta < 26°$; third, we suspect that other physical effects, like electrolysis, will become active at high V/low θ, and this snap-to total wetting will not occur.

of vacuum, and an applied voltage of 100 V the ratio of the interfacial to electrical energies is approximately $a/2W = a/2R\epsilon_l V^2/R^2 \gamma_{lg} = a/2\epsilon_l V^2/R \gamma_{lg} \approx (0.06/2) \times (2.5 \times 8.85 \times 10^{-12}$ C/Vm$) \times (100$ V$)^2/(0.0001$ m$) \times (0.02$ J/m$^2)$ $= 0.0033$. Evidently, less than 1% of the energy of our example drop is electrical energy. We would have to increase the voltage up to 1000 V before the electrical energy becomes appreciable; in that case $a/2W \approx 0.4$.

Creating such a high voltage for such a small drop could lead to dielectric breakdown: the electric field generated for 1000 V across a 0.1 mm drop is $|\mathbf{E}| \sim V/R = 10^7$ V/m. For oils, dielectric breakdown typically occurs right around 10^7 V/m. In terms of the electric field, the electro-wetting number W scales as $\epsilon_l R^2 (V/R)^2/R \gamma_{lg} = \epsilon_l R |\mathbf{E}|^2/\gamma_{lg}$, so it would actually make more sense to pick an electric field that is high but is substantially below the dielectric breakdown, and then to increase the drop radius R until W approaches unity. Such an experiment should allow one to see appreciable line-tension effects.

3. Young's equation for a dielectric liquid: The "line-tension" term

Applying Eq. (15) to Eq. (23) and dividing by γ_{lg}, gives the nondimensional Young equation for a dielectric liquid drop in terms of the electro-wetting number $W = \epsilon_l V^2/R \gamma_{lg}$

$$\cos\theta - \left(\frac{\gamma_{gs} - \gamma_{ls}}{\gamma_{lg}}\right) - \frac{1}{2}\left(\frac{\epsilon_l V^2}{R\gamma_{lg}}\right)\left[-\frac{2 + \cos\theta}{2\pi\sin\theta}\right]$$
$$\times\left[a_{de}(\theta)q(\theta) + \frac{da_{de}}{d\theta}(\theta)\right] = 0. \qquad (24)$$

Here $q(\theta)$ is defined immediately below Eq. (4) and $a_{de}(\theta)$ is shown in Fig. 5. Notice the $1/R$ "line-tension" dependence. We write "line tension" in quotes because the effect

is not, in fact, due to a line tension in any physical sense. It arises because the drop volume scales as R^3 and the electric field scales as V/R. Upon integration of the dielectric energy this gives an R-type energy dependence, which becomes a $1/R$ force dependence via Sec. III C, Eq. (15). The exact same scaling argument gives, for a conducting drop on an insulating surface, and R^2 energy dependence in Eq. (17) and no $1/R$ line tension in Eq. (18).

Equation (24) cannot be solved analytically, but can be solved numerically. Figure 6 shows the resulting variation in contact angle as a function of the nondimensional electro-wetting parameter $W = \epsilon_l V^2/R \gamma_{lg}$. The contact angle decreases only gradually with increasing W. This means that dielectric liquids on conducting solids will change shape only slightly under applied electric fields. It is clear why it would be difficult to measure such an effect experimentally: the effect is small and it is sensitive to the dielectric properties of the liquid.

C. Slightly resistive liquid atop a dielectric, highly-resistive solid implies contact angle saturation

In Sec. IV A we considered the case of a conducting liquid atop a perfectly insulating dielectric solid: this case recovered the Young–Lippmann Eq. (18), and was a first-cut model of the physical situation encountered in our electro-wetting devices. However, the assumption of a perfect insulator is unrealistic, and so we introduce the resistance of the solid (which is large by design) and also a small amount of liquid resistance (which is unavoidable in practice). Liquid resistivity depends on the number and type of ions in the
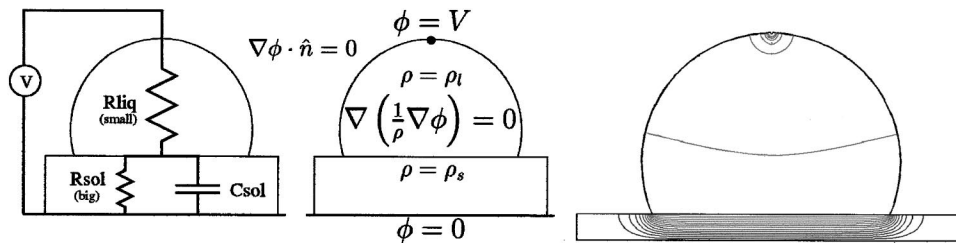
FIG. 7. Left: A bulk circuit diagram for a liquid with a small amount of electrical resistance R_{liq}, atop a dielectric solid with capacitance C_{sol} and a large amount of electrical resistance R_{sol} (by design). Middle: The corresponding (steady-state) PDE with boundary conditions. Here, $\phi(x,y,z)$ is the electric potential inside the three-dimensional drop; ρ is the resistivity (units Ω m) where $\rho=\rho_l$ inside the liquid is small and $\rho=\rho_s$ inside the solid is large, and $\nabla(1/\rho\nabla\phi)=0$ includes the liquid/solid electric field jump conditions; $\hat{n}$ is the outward unit normal and so $\nabla\phi\cdot\hat{n}=0$ is the no-flux external boundary condition; finally $\phi=V$ and $\phi=0$ are the top and bottom boundary conditions applied by the voltage source. Right: This figure shows an example solution of the PDE equations. The lines show 28 equally spaced contours of constant $\phi(x,y,z)=c$ for a vertical slice through the three-dimensional liquid and solid geometry. Notice that almost all the voltage drop occurs across the solid but there is also a small amount of voltage drop in the liquid.

liquid, see Probstein,[12] Sec. 2.5. These features are all that is required to replicate the contact angle saturation that we see in our devices.

We note that many different physical effects can potentially cause contact angle saturation. Any kind of loss mechanism will cause the reversible dielectric energy stored in the solid to deviate away from the ideal Young–Lippmann value. Verheijen and Prins[5] present a convincing argument that charge trapping is the dominant loss mechanism in their devices. Other mechanism are proposed in Refs. 4,6 and 24. We stress three points here. One, a reasonable amount of liquid resistance will cause contact angle saturation (see the development below). Two, the saturation predicted by liquid resistance accurately matches the experimental data we see in our devices (see Fig. 13). Three, liquid resistance is the leading cause of contact angle saturation in our devices. We examined a large number of physical mechanisms and liquid resistance was the only physically meaningful assumption that was able to explain our experimental data.

1. Equivalent circuit diagram

To understand how liquid resistance affects contact angle saturation, first consider the bulk circuit diagram shown on the left side of Fig. 7. When the total resistance is large but finite, there is a small amount of current flow I through the liquid and solid. Following standard electrical engineering practice, the relation between the voltage V and the current I is most conveniently expressed in the frequency domain by a complex impedance $z(s)=V(s)/I(s)$. (Here s is the Laplace variable. For a sinusoidal signal $V(t)=\bar{V}\cos(wt)$ of frequency w, take $s=iw$. Setting $w=0$ gives back the steady-state $V(t)=\bar{V}$ case.) The total impedance for the circuit diagram shown in Fig. 7 is

$$\frac{V(s)}{I(s)}=z(s)=\frac{1+\dfrac{R_{\text{liq}}}{R_{\text{sol}}}+sR_{\text{liq}}C_{\text{sol}}}{sC_{\text{sol}}+\dfrac{1}{R_{\text{sol}}}}. \qquad (25)$$

If the liquid resistance is set to zero ($R_{\text{liq}}\to 0$) and the solid resistance is set to infinity ($R_{\text{sol}}\to\infty$) to model a perfect in-

sulator, then the above impedance $z(s)$ reduces to $z(s)=1/sC_{\text{sol}}$ and we recover the pure solid capacitive case of Sec. IV A.

As before, all the reversible electrical energy is stored in the solid capacitor and the voltage source. (The liquid and solid resistance only cause a non-reversible energy loss.) The energy stored in the solid capacitor is still $E_{\text{de}}=\frac{1}{2}C_{\text{sol}}V_{\text{sol}}^2$, where V_{sol} is the voltage drop across the solid (see Feynman,[33] Vol. II, Chap. 22, Sec. 5). To find this voltage drop, note that the impedance of the solid is $z_{\text{sol}}=1/(1/sC_{\text{sol}}+1/R_{\text{sol}})$, that the current through the liquid is the current through the solid is the total current $I_{\text{liq}}=I_{\text{sol}}=I$, and that Eq. (25) relates $V(s)$ and $I(s)$, hence

$$V_{\text{sol}}(s)=z_{\text{sol}}(s)I(s)=\frac{z_{\text{sol}}(s)}{z(s)}V(s)$$

$$=\left(\frac{1}{1+\dfrac{R_{\text{liq}}}{R_{\text{sol}}}+sR_{\text{liq}}C_{\text{sol}}}\right)V(s). \qquad (26)$$

Thus in steady state, i.e., as $s=iw\to 0$, the voltage and energy stored in the dielectric are

$$\bar{V}_{\text{sol}}=\left(\frac{1}{1+\dfrac{R_{\text{liq}}}{R_{\text{sol}}}}\right)\bar{V},\quad \bar{E}_{\text{de}}=\frac{1}{2}C_{\text{sol}}\left(\frac{1}{1+\dfrac{R_{\text{liq}}}{R_{\text{sol}}}}\right)^2\bar{V}^2,$$

$$(27)$$

where $\bar{V}$ is the applied dc voltage. This is the same dependence as shown in Eq. (16) for the perfectly insulating solid (since $C_{\text{sol}}=\epsilon_s A_{\text{ls}}/h$), except for the new $R_{\text{liq}}/R_{\text{sol}}$ term. The key observation is that the resistance of the liquid drop R_{liq} is shape dependent, and it is this dependence of the resistance on the contact angle $R_{\text{liq}}=R_{\text{liq}}(\theta)$ that is going to lead to contact angle saturation. The mechanism is elucidated below.

2. PDE's and their solution

Our first task is to find the PDE's and boundary conditions that describe the steady-state electric potential $\phi(x,y,z)$ inside the liquid and the solid.

We have assumed that the liquid is a resistor with resistivity ρ_l but that it has no capacitive effects. The current
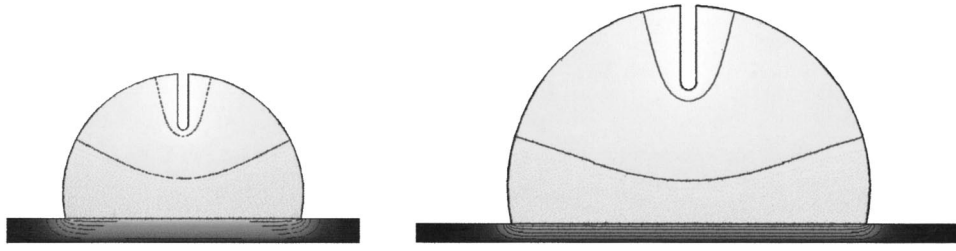
FIG. 8. Solution scaling: Both pictures show the electric potential inside the liquid and solid with the same color scale: white denotes high electric potential, black denotes zero potential, and the curves denote surfaces of constant $\phi(x,y,z)$. The notch at the top represents the inserted wire electrode: the wire insertion depth D is fixed and is taken into account in the scaling argument. The picture on the left shows a solution of Eq. (28) with $R_o = 1$, $h = 0.2$ and $\bar{A}_o = 0.2\rho_s/\rho_l = 10$. The picture on the right shows a solution for $R_o = 1.5$, $h = 0.15$ and the same liquid/solid resistance ratio $\bar{A}_o = 0.15\rho_s/1.5\rho_l = 10$. Notice that the solutions are essentially self-similar. There is a small discrepancy because the scaling argument ignores the horizontal stretching of the electrical edges effects in the solid region immediately underneath the triple line.

density in the liquid is given by $\mathbf{j}_l = \mathbf{E}/\rho_l$ where $\mathbf{E}$ is the local electric field. By comparison, the solid has both a resistive and capacitive component with resistivity ρ_s and dielectric constant ϵ_s. The instantaneous current density in the solid is given by $\mathbf{j} = \mathbf{E}/\rho_s + \epsilon_s d\mathbf{E}/dt$. At steady state, the $d\mathbf{E}/dt$ term goes to zero and we are left with $\mathbf{j} = \mathbf{E}/\rho_s$. Conservation of charge states that the divergence of the current density is zero: $\nabla \mathbf{j} = 0$. Moreover, the electric field is minus the gradient of the electric potential $\mathbf{E} = -\nabla \phi$ hence

$$\nabla\left(\frac{1}{\rho}\nabla\phi\right) = 0, \quad \rho = \begin{cases} \rho_l & \text{resistivity in the liquid} \\ \rho_s & \text{resistivity in the solid} \end{cases} \quad (28)$$

is the PDE that describes the electric potential inside both the liquid and the solid at steady-state. This formulation correctly includes the conservation of current flow in the vertical direction across the solid/liquid interface, namely: $j_z = (\partial\phi/\partial z)/\rho$ is a constant across the interface with $\rho = \rho_l$ in the liquid and $\rho = \rho_s$ in the solid, hence the solid/liquid jump conditions are $\rho_s \partial\phi_l/\partial z = \rho_l \partial\phi_s/\partial z$.

Boundary conditions for Eq. (28) are as follows. The potential at the bottom of the solid is fixed at a nominal (and arbitrary) $\phi = 0$ potential. An inserted electrode at the top of the liquid is held at $\phi = V$ by the applied voltage source. At all the liquid/gas and solid/gas boundaries we use a zero normal electric field condition $\mathbf{E} \cdot \hat{n} = \nabla\phi \cdot \hat{n} = 0$, where $\hat{n}$ is the outward unit normal. This last condition is analogous to the liquid/gas jump condition, here $(\rho_{l/s}/\rho_g)\mathbf{E}_g \cdot \hat{n} = \mathbf{E}_{l/s} \cdot \hat{n}$, except that we further assume that the resistivity of air ρ_g is large compared to the resistivity of the liquid ρ_l and solid ρ_s, and so $\mathbf{E}_{l/s} \cdot \hat{n}$ is essentially zero at the liquid/gas and solid/gas boundary.

A summary of the PDE and its boundary conditions is shown in the middle of Fig. 7. The right side of the figure shows a sample solution for a $\theta = 114°$ contact angle with applied voltage $V = 1$, liquid radius $R = 1$, solid height $h = 0.2$, and resistivity ratio randomly chosen at $\rho_s/\rho_l = 230$. This solution should be understood as follows: if the drop shape were to somehow be held at $\theta = 114°$ and a voltage $V = 1$ were suddenly applied, the electric potential $\phi(x,y,z)$ inside the liquid and solid would approach the field lines shown on the right side of the figure at a rate of $1/\tau$. This time constant τ is the charging time for the solid capacitor

based on the available current flow through the liquid and solid. From the preceding section, it can be shown and then estimated that

$$\tau = \frac{C_{\text{sol}}}{1/R_{\text{sol}} + 1/R_{\text{liq}}} \approx \frac{\epsilon_s R^2/h}{R^2/\rho_s h + R/\rho_l}. \quad (29)$$

For a $R = 1$ mm water drop, with $\rho_l \approx 5 \times 10^4$ Ω m, $\rho_s \approx 10^{12}$ Ω m, $\epsilon_s = 16 \times 10^{-12}$ C/Vm [39] and solid height $h = 10^{-6}$ m, this time-constant τ is on the order of 10^{-3} s. Because this time constant is quite fast, it is reasonable to treat the potential $\phi(x,y,z)$ as a steady-state quantity. Once the potential ϕ is known, the dielectric energy stored in the system is given by the integral of $dE_{\text{de}} = \frac{1}{2}(\mathbf{D} \cdot \mathbf{E})dv = \frac{1}{2}(\epsilon_s \nabla\phi) \cdot (\nabla\phi)dv$ over the solid geometry

$$E_{\text{de}}(R, \theta, h, V, \rho_s/\rho_l, \epsilon_s) = \frac{1}{2}\int_{\text{sol}} \epsilon_s |\nabla\phi(x,y,z)|^2 dv. \quad (30)$$

Equation (30) mathematically captures the contact angle shape dependence left unsaid in Eq. (27). As previously, the total electrical energy is the sum of the energy stored in the dielectric and in the voltage source: $E_{\text{elec}} = E_{\text{de}} + E_{vs} = E_{\text{de}} - 2E_{\text{de}} = -E_{\text{de}}$.

3. Electrical energy scaling

Equation (30) shows how the electrical energy depends on the geometry (R, θ, h), the applied voltage V, and the material properties ρ_s/ρ_l and ϵ_s. Our task now is to flush out and simplify this dependence so that we can understand how the energy minimum varies with geometry, applied voltage, and material properties. This can be done by a scaling analysis just like the one used in Secs. III B, IV A 1, and IV B 1, but with one additional key assumption.

If we look at the electric potential solution shown on the right of Fig. 7, we see that the potential field surfaces $\phi_s(x,y,z) = c$ inside the solid are horizontal except right below the drop edges. This is because the height of the solid, $\bar{h} = 0.2$, is small compared to the radius of the liquid $\bar{R}$. In our electro-wetting devices $h/R < 10^{-4}$, hence the energy content of the edge effects is tiny, and we can assume the electric field in the solid is essentially vertical: $\mathbf{E}_s \approx -(0,0,\partial\phi_s/\partial z)$.

Then the basic scaling result is this. If we take an existing solution to Eq. (28) with the boundary conditions of Fig. 7, and we stretch the liquid in the x, y, z directions by a factor $\hat{R}$, and stretch the solid by a factor $\hat{R}$ in the x, y directions, and by $\hat{h}$ in the z direction, the end result is still a solution so long as the resistance of the liquid or solid is also changed so as to keep the resistance ratio $\bar{A}_0 = h\rho_s/R_o\rho_l$ at its previous value. Figure 8 shows this scaling idea graphically.

This means that if we know the solution to Eq. (28) with the boundary conditions of Fig. 7 for a fixed liquid radius $\bar{R}=1$, solid height $\bar{h}=0.2$, applied voltage $\bar{V}=1$, and for any contact angle $\bar{\theta}$, any normalized electrode penetration depth $\bar{D}/\bar{R}$ and any resistivity ratio $\bar{\rho}_s/\bar{\rho}_l = \bar{A}$, then we also know the solution for any combination of parameters $R, h, D, V, \theta, \rho_s$ and ρ_l. We are going to assume that the electrode is always at a fixed height H above the solid because this is how the experiment is actually done. Thus the relation between the radius R, contact angle θ and the electrode penetration depth D is $D = 1 - \cos\theta - H/R$ where H is fixed but R, θ and D vary. (The electrode insertion depth D is shown in Fig. 8 but not in Fig. 7.) Using this relation $D = D(R, \theta)$ we can suppress further discussion of the D parameter. In mathematical terms, if we let $\bar{\phi}^{\theta,\bar{A}}(\bar{x},\bar{y},\bar{z})$ be the known solution for $\bar{R}=1, \bar{V}=1$ and $\bar{h}=0.2$, (and choose z such that $z=0$ at the solid/liquid interface) then

$$
\phi(x,y,z)=
\begin{cases}
\phi_l(x,y,z)=V\bar{\phi}_l^{\theta,\bar{A}}\left(\dfrac{x}{R},\dfrac{y}{R},\dfrac{z}{R}\right) & \text{in the liquid} \\[2em]
\phi_s(x,y,z)=V\bar{\phi}_s^{\theta,\bar{A}}\left(\dfrac{x}{R},\dfrac{y}{R},\dfrac{\bar{h}z}{h}\right) & \text{in the solid}
\end{cases}
\tag{31}
$$

is a solution for arbitrary R, h, V, θ, ρ_s, and ρ_l where $\bar{A}$ must be set to $\bar{h}\bar{A}=\rho_s h/\rho_l R$. For example, to find a solution for $R=1$ mm, $h=0.2\ \mu$m, $V=50$ V, $\theta=120°$, and $\rho_s/\rho_l = 327$, we first find the nondimensional solution $\bar{\phi}$ for $\bar{R}=1$, $\bar{h}=0.2$, $\bar{V}=1$, $\bar{\theta}=120°$, and $\bar{A}=0.327$, then the dimensional solution is given by Eq. (31). (For a proof of this statement, see the Appendix.)

Using the above scaling, and noting once again that the total electric energy is minus the energy stored in the dielectric (see Secs. IV A 2 and IV A 3), we find that the total electric energy is given by

$$
E_{\text{elec}}(R,\theta,h,V,\rho_s/\rho_l,\epsilon_s)
$$

$$
= -\frac{1}{2}\int_{R,h\ \text{solid}}\epsilon_s|\nabla\phi(x,y,z)|^2 dv
$$

$$
= -\frac{1}{2}\left(\frac{\epsilon_s R^2}{h}\right)V^2\bar{h}
$$

$$
\times \int_{\bar{R}=1,\bar{h}=.2\ \text{solid}}\left|\nabla\bar{\phi}_s(\bar{x},\bar{y},\bar{z})\right|_{\theta,\bar{A}=\frac{\rho_s h/\bar{h}}{\rho_l R}}^2 d\bar{v}
$$

$$
= -\frac{1}{2}\left(\frac{\epsilon_s R^2}{h}\right)V^2\bar{h}a\left(\theta,\frac{\rho_s h/\bar{h}}{\rho_l R}\right).
\tag{32}
$$

By using scaling arguments, we have managed to take an energy that depends on six variables $(R,\theta,h,V,\rho_s/\rho_l,\epsilon_s)$, and rewritten it in terms of two nondimensional numbers $(\theta,\bar{A})$ times a simple dimensional quantity $(\epsilon_s R^2 V^2/h)$. It remains to find the shape factor $a(\theta,\bar{A})$. We do this numerically in the next section.

4. Shape factor $a(\theta,\bar{A}(R))$ and the constant volume energy minimum

At this stage, we are within the energy minimization framework outlined in Sec. II. For our slightly resistive drop atop a highly resistive solid, we could note that the total energy of the drop $E(R,\theta)$ is given by a sum of the interfacial energy $E_{\text{int}}(R,\theta;p_1)$ in Eq. (10), and the electrical energy $E_{\text{elec}}(R,\theta;p_2)$ in Eq. (32). We could then compute $a(\theta,\bar{A})$ numerically and solve Eq. (5) with outside parameters $p_1 = (\gamma_{\text{ls}}-\gamma_{\text{gs}},\gamma_{\text{lg}})$ and $p_2 = (h,V,\rho_s/\rho_l,\epsilon_s)$. This would yield the equilibrium contact angle θ as a function of R, p_1 and p_2.

However, this process is tedious for the following reason. The shape factor $a(\theta,\bar{A})$ here depends on two variables. To map it out accurately we would have to evaluate a for at least 15 values of θ and 10 values of $\bar{A}$. This is 150 solutions of the three-dimensional PDE Eq. (28). To get a sufficiently fine-scale solution takes about 15 min per simulation, which is a total of 37.5 h of run time. (Of course we could parallelize the computations, and take previous solutions as initial conditions for subsequent solution, but still, doing it in this way is a significant computational burden.)

Instead, we are going to use a short-cut. The volume $v = v(R,\theta)$ of the liquid drop is fixed. Inverting Eq. (2) yields

$$
\frac{R(\theta)}{R_o}=r(\theta)=\sqrt[3]{\frac{4/3}{\dfrac{2}{3}-\dfrac{3\cos\theta}{4}+\dfrac{\cos 3\theta}{12}}},
\tag{33}
$$

where $R_o = \sqrt[3]{3v/4\pi}$ is the nominal radius of a drop of volume v that is a perfect sphere (so for $\theta=\pi$). Under the constant volume constraint, the shape factor a only has a θ dependence

$$
a(\theta)=a\left(\theta,\frac{\rho_s h/\bar{h}}{\rho_l R(\theta)}\right)=a\left(\theta,\frac{\bar{A}_o}{\bar{h}r(\theta)}\right)
\tag{34}
$$

with $\bar{A}_o = \rho_s h/\rho_l R_o$. Using this relation for the radius R in terms of θ, the total energy can be written in nondimensional form as

$$
\frac{E(\theta)}{\gamma_{\text{lg}}R_o^2}=r^2(\theta)\left[\left(\frac{\gamma_{\text{ls}}-\gamma_{\text{gs}}}{\gamma_{\text{lg}}}\right)\pi\sin^2\theta+2\pi(1-\cos\theta)\right]
$$

$$
-\frac{1}{2}\left(\frac{\epsilon_s V^2}{h\gamma_{\text{lg}}}\right)r^2(\theta)\left[\bar{h}a\left(\theta,\frac{\rho_s h}{\rho_l R_o}\frac{1/\bar{h}}{r(\theta)}\right)\right].
\tag{35}
$$

Notice the dependence on the three nondimensional parameters

$$
\Gamma=\frac{\gamma_{\text{ls}}-\gamma_{\text{gs}}}{\gamma_{\text{lg}}}=\text{nondimensional surface tension coefficient,}
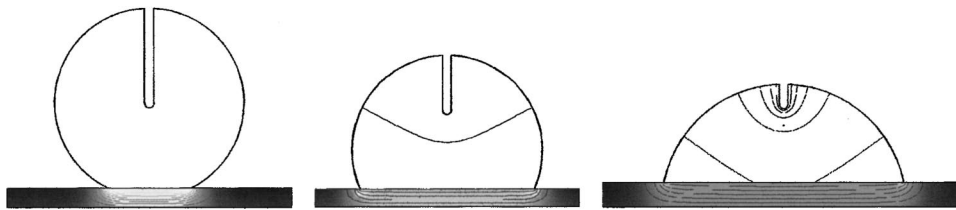$$

FIG. 9. The strength of the electric field inside the solid, and thus the amount of stored electrical energy, decreases as the liquid drop approaches total wetting. Here we show a case where the resistivity of the liquid is 50 times smaller than the resistivity of the solid. All scaling is according to Eq. (31), but with the figures drawn to show a constant electrode height. The solid is colored by the strength of its electric field $|\nabla\phi_s|$, with black denoting a low electric field, light gray up to white representing a high field. Notice how the electric field strength in the solid decreases as the droplet spreads and there is a progressively longer liquid path from the bottom of the top electrode to the solid near the triple line. (If there was no liquid resistance, the size of electric field in the solid would remain the same for all contact angles.)

$$U = \frac{\epsilon_s V^2}{h\,\gamma_{\mathrm{lg}}} = \text{electro-wetting number for dielectric solid,}$$

$$\bar{A}_o = \frac{\rho_s h}{\rho_l R_o} = \text{solid/liquid resistivity ratio.}$$

These three nondimensional parameters will uniquely determine the contact angle.

Figure 9 shows sample potential field solutions $\phi(x,y,z)$ for $\bar{A}_o = 10$ for three values of θ. Here the solid is colored by the magnitude of the local electric field $|\nabla\phi_s(x,y,z)|$. The constant liquid volume shape factor $\bar{h}a[\theta,\bar{A}_o/\bar{h}r(\theta)]$ is now computed by numerically integrating $|\nabla\phi_s(x,y,z)|$ over the solid (edge effects are truncated). Results are plotted against θ for four values of $\bar{A}_o$ in Fig. 10. As is necessary, the zero liquid resistance (infinite $\bar{A}_o$ case) reduces to the Sec. IV A scenario with $\bar{h}a(\theta,1000/\bar{h})$ indistinguishable from $\pi\sin^2\theta$ [compare with Eq. (16)]. As the resistance is increased, the form factor a begins to fall away from the zero resistance case, reflecting the fact that there is now a substantial voltage drop across the liquid and less capacitive energy is being stored in the solid.

5. Detailed explanation of contact angle saturation

We can now precisely explain contact angle saturation through Figs. 11 and 12.

Figure 11 shows the net electrical energy (when $\frac{1}{2}U = 1$) as a function of the contact angle θ for a liquid drop of
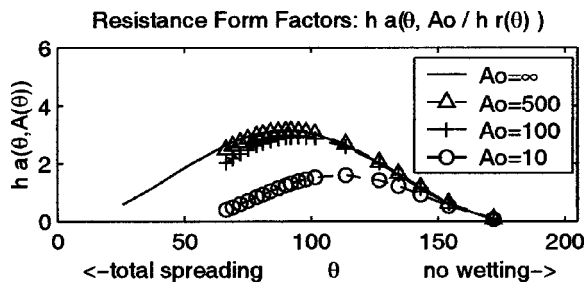

FIG. 10. The constant liquid volume shape factor of Eqs. (32) and (34). If there is no liquid resistance, the form factor is proportional to the liquid/solid area: $a(\theta,\infty) = \pi\sin^2\theta$. As the liquid resistance increases (A_o decreases) the energy stored in the solid falls away from the ideal zero liquid resistance case. Points on the graph above are found by a numerical solution of Eq. (28). When θ reaches 66° the top of the liquid drop has fallen below the bottom tip of the inserted electrode: this effect can be seen in Fig. 9.

constant volume. Different curves are shown for four values of the solid to liquid resistance ratio $A_o = \rho_s h/\rho_l R_o$. The solid/liquid interface energy curve $E_{\mathrm{sl}}(\theta)$ is shown for comparison. For zero liquid resistance, the $A_o = \infty$ curve is the mirror image of the E_{sl} curve: $E_{elec}(\theta) = -E_{\mathrm{sl}}(\theta)$. In this case, Eq. (35) becomes

$$E = \Gamma E_{\mathrm{sl}} + E_{\mathrm{lg}} - \tfrac{1}{2}UE_{\mathrm{sl}} = \left(\Gamma - \tfrac{1}{2}U\right)E_{\mathrm{sl}} + E_{\mathrm{lg}}. \tag{36}$$

It is as if the applied voltage in $U = \epsilon_s V^2/h\gamma_{\mathrm{lg}}$ were directly changing the surface tension coefficients in $\Gamma = (\gamma_{\mathrm{ls}} - \gamma_{\mathrm{gs}})/\gamma_{\mathrm{lg}}$. So this says that if we increase U high enough (up to $\Gamma - \tfrac{1}{2}U = -1$) then we would drive the contact angle to $\theta = 0$. The left side of Fig. 12 shows this scenario notice how as U increases, the energy curve unbends, and at $U = 3$ (when $\Gamma - \tfrac{1}{2}U = \tfrac{1}{2} - \tfrac{1}{2}\times 3 = -1$) the contact angle arrives smoothly at total spreading.

But there is always some liquid resistance: $A_o \neq \infty$. As this liquid resistance increases (A_o decreases) the electrical energy $E_{\mathrm{elec}}(\theta,A_o)$ deviates away from the ideal $-E_{\mathrm{sl}}(\theta)$ value as shown in Fig. 11. This is just a consequence of
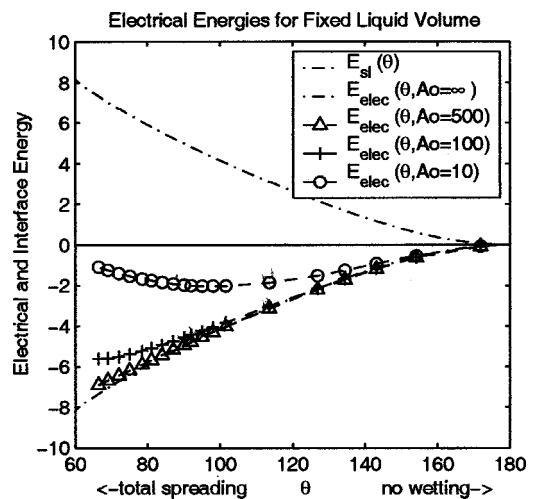

FIG. 11. This figure shows electrical energy curves for a fixed liquid volume. When there is no liquid resistance ($A_o = \infty$), the electrical energy exactly balances the solid/liquid interfacial energy: $E_{\mathrm{elec}}(\theta,A_o = \infty) = -(2\Gamma/U)E_{\mathrm{ls}}(\theta)$. This implies that the imposed electric energy can perfectly cancel the energy due to the liquid/solid interface. When the liquid resistance is nonzero ($A_o < \infty$), the electric energy deviates away from the mirror image of E_{sl} and it is not possible to cancel the effect of the solid/liquid energy by driving up the voltage. This leads to the contact angle saturation shown in Figs. 12 and 13.
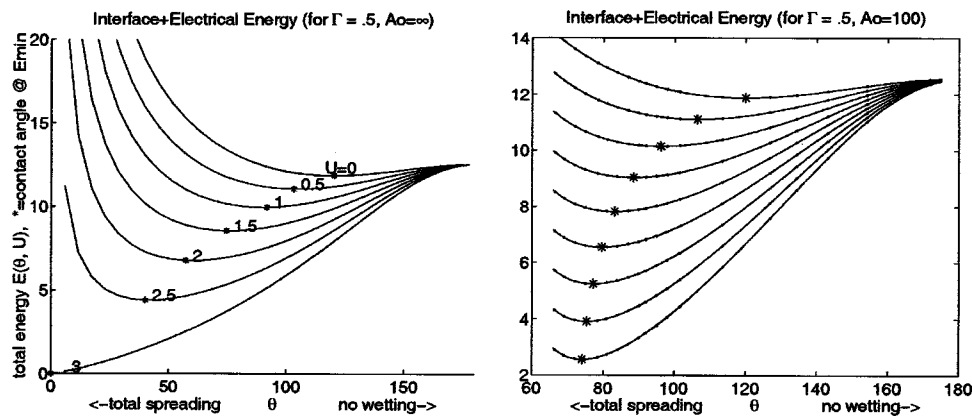
FIG. 12. Left: Total energy curves for a constant liquid volume as a function of contact angle θ when the liquid resistance is zero. Different curves correspond to different electro-wetting numbers $U = \epsilon_s V^2 / h \gamma_{lg} = [0, 0.5, \ldots, 2.5, 3]$. The contact angle slides smoothly to zero as U increases. Right: The same plot, now including a small amount of liquid resistance: $A = \rho_s h / \rho_l R_o = 100$. At lower contact angles, there is a greater net liquid resistance, hence there is a greater energy loss, and hence the applied electric field cannot drive the contact angle to zero. Consequently, the contact angle is caught in an energy minimum around $\theta \approx 75°$.

solving Maxwell's Eq. (28) with the boundary conditions of Fig. 7 and using the constant liquid volume constraint of Eq. (33). This numerical result can be explained intuitively. As θ decreases, the radius of the drop increases (to keep the volume constant) and in addition the liquid edges pull away from the fixed electrode (as shown in Fig. 9) this means that the ions in the liquid have to travel a longer distance to get from the electrode at the top to the solid at the bottom. Thus the effective resistance of the liquid increases as contact angle decreases. For greater liquid resistivities ρ_l, the resistance first starts to increase appreciably at larger contact angles θ.

We note that even a small amount of liquid resistance implies that it is not possible to drive the contact angle to zero with an applied voltage of any size. For a fixed volume, the interfacial area, and hence the energy, of Eq. (35) goes to infinity as contact angle goes to zero at a rate of $r(\theta)$

$\sim \theta^{-2/3}$ due to an area versus volume scaling argument. But the electrical energy goes to infinity at a slower rate due to the $1/r(\theta)$ term inside the shape factor a in Eq. (35). Hence for sufficiently small θ, the interfacial energy will always beat the electrical energy, the total energy will go to infinity as θ goes to zero, and so $\theta = 0$ can never be an energy minimum, no matter the applied voltage.

V. CONTACT ANGLE SATURATION MODEL VERSUS EXPERIMENTS

The experimental setup is as shown in Fig. 2. For the experiments cited here, the insulating dielectric layer consists of either a single layer of Teflon or a double layer of Teflon and silicon dioxide (see Fig. 13). Silicon is used for the bottom electrode, and a metal wire is employed for the top inserted electrode. More experimental details can be
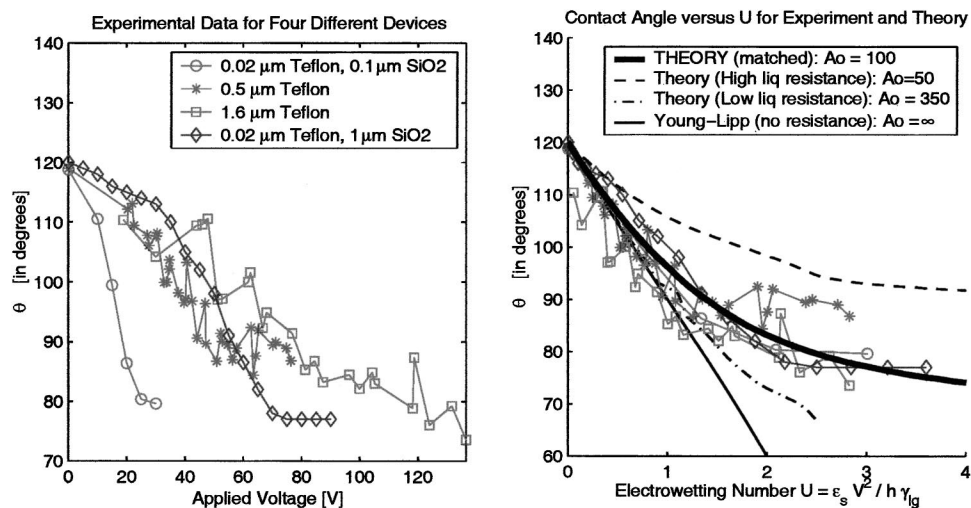

FIG. 13. Left: Measured contact angle vs applied voltage for four different Teflon/silicon oxide coatings. Right: The same data is re-plotted against the nondimensional electro-wetting number $U = \epsilon_s V^2 / h \gamma_{lg}$. The thin solid line shows the Young–Lippmann prediction. The two dashed lines show our theory for a low and high liquid resistance. The thick solid line shows our prediction when we take the resistance ratio $A_o = 100$. Since for our experiments $h/R \sim 10^{-4}$, this corresponds to a liquid resistivity 10^{-6} times smaller than the solid resistivity. We have not yet been able to measure A_o experimentally (we have to measure the resistance across the solid and in the liquid) but $A_o = 100$ is of the right order of magnitude for our high resistance dielectric coatings.

TABLE I. Summarizes the examples of Sec. III. For each physical effect: column two lists the energy associated with that effect; column three shows the resulting term that appears on the right-hand side of Young's equation; and column four gives the relevant nondimensional number. For example, the ratio between surface tension and gravity forces is given by the bond number B. If there are many competing effects, then each effect will enter with a size corresponding to its nondimensional number.

Physical effect	Resulting energy term: $E(R, \theta, p_1, p_2, \dots) =$	Term on right in Young: $\cos\theta = \dots$	Nondimensional number	Comments
Interfacial energy	$(\gamma_{ls} - \gamma_{gs})A_{ls} + \gamma_{lg}A_{lg}$ see Eqs. (8), (9), (10)	$\cos\theta = -\Gamma$	$\Gamma = \dfrac{\gamma_{ls} - \gamma_{gs}}{\gamma_{lg}}$	Exactly recovers Young's equation
Gravity	$R^4 \varrho g \dfrac{2\pi}{3}[3 + \cos\theta]\sin^6\left(\dfrac{\theta}{2}\right)$	$-B\left[\dfrac{\cos\theta}{3} - \dfrac{\cos 2\theta}{12} - \dfrac{1}{4}\right]$	$B = \dfrac{R^2 \varrho g}{\gamma_{lg}}$	Usually small
Dielectric solid	$-\dfrac{\epsilon_s V^2 A_{ls}}{2h} = -\dfrac{\epsilon_s V^2}{2h}R^2\pi\sin^2\theta$ see Eqs. (16) and (17)	$+\dfrac{1}{2}U$	$U = \dfrac{\epsilon_s V^2}{h\gamma_{lg}}$	Recovers the Lipp–Young Eq.
Ion layer capacitance	$-\dfrac{\epsilon_l A_{ls} V_{dl}^2}{2\lambda_D} \geqslant -\dfrac{\epsilon_l A_{ls}}{2\lambda_D}\left[\dfrac{2\lambda_D \epsilon_s}{h\epsilon_l}V\right]^2$ V_{dl} voltage across ion layer	$\leqslant \dfrac{1}{2}U \times 4D$	$D = \dfrac{\lambda_D \epsilon_s}{h\epsilon_l}$ very small	Is negligible, see Sec. IV A 4
Dielectric liquid	$-\dfrac{1}{2}\epsilon_l R V^2 a_{de}(\theta)$ See Eq. (22), Fig. 5	$+\dfrac{1}{2}Wb(\theta)$ for b, see Eq. (24)	$W = \dfrac{\epsilon_l V^2}{R\gamma_{lg}}$	Note the $\dfrac{1}{R}$ line tension in W
Liquid resistance	$-\dfrac{\epsilon_s A_{ls}}{2h}\left(\dfrac{V}{1 + R_{liq}/R_{sol}}\right)^2$ $= -\dfrac{\epsilon_s R^2 V^2}{2h}a(\theta, \bar{A}_o/R)$	Not found explicitly, see Sec. IV C 4.	$\bar{A}_o = \dfrac{\rho_s h}{\rho_l R_o}$ is large	Liquid resistance leads to contact angle saturation

found in Moon *et al.*[24] Experimental results are shown on the left of Fig. 13. Results are plotted for four different coatings as contact angle versus voltage.

The first step is to re-plot this data against the nondimensional electro-wetting number $U = \epsilon_s V^2 / h\gamma_{lg}$ of Eq. (35), then, as seen on the right of the figure, all the data essentially fall on a single master curve. The theory we have developed in the preceding sections predicts this master curve. We are able to match all the data if we take a solid/ liquid resistance ratio of $\bar{A} = 100$. Since the liquid radius in our devices is on the order of 10 000 times greater than the solid thickness h, this corresponds to a liquid/solid resistivity ratio $\rho_l/\rho_s \sim 10^{-6}$: this is all that is necessary to cause a 75 ° contact angle saturation.

VI. RESULTS SUMMARY

a. *Minimum total energy and Young's equation*: All the results in this article are based on a minimum energy framework. This in itself is not new, see Chap. 10 in Probstein,[12] and Refs. 15, 16, and 26 for example. However, we have made a careful effort to extract as much information from the energetics framework as is possible. We have explicitly included size dependence in the energy minimum formulation, and have found an analytic relation between the change in contact angle $d\theta$ and the change in radius dR necessary to keep the liquid volume constant [see Eqs. (2) and (4)]. This leads to Eq. (6) which is in fact exactly Young's equation if we consider the energy due to interfacial effects only (see

Sec. III A); but it further allows the inclusion of any other energy terms (due to gravity, capacitive effects, the double layer, etc.). Specifically, we have found a simple and interesting link between energy scalings and the associated terms in Young's equation. Any physical effect that gives rise to a $E \propto R^k$ energy size dependence, will give a R^{k-2} term in Young's equation (see Sec. III C).

b. *Summary of physical examples*: Table I summarizes the examples of Sec. III.

c. *A triple-line force balance is insufficient*: Much of the early literature analyzed surface tension by phrasing a force balance at the triple line only (see Fig. 14) The limitation of this viewpoint has been recognized in some recent articles.[5,6,26] Essentially, if we have internal bulk forces as occur in the case of gravity (the simplest example) or because of internal electric fields such as the one shown in Fig. 4, then we must balance the bulk volume forces against the interfacial effects. To do so, one must either consider the forces everywhere (not just at the triple line) or one must

FIG. 14. The left diagram shows a force balance at the triple line only. This model cannot capture the effect of internal forces (shown schematically on the right) such as gravity or the forces due to internal electric fields. For example, the electric field of Sec. IV B, Fig. 4 will create forces everywhere inside the liquid.

minimize the total system energy as we have done here.

d. *Only consider gross liquid shape*: We have ignored local details of the liquid shape, meaning we do not account for liquid pinching at the top electrode or for the details of the shape at the three phase line. Instead, we have assigned two numbers R and θ which parametrize the gross shape of the liquid drop as shown in Fig. 1. For all the different physical scenarios discussed in Sec. III, at the end we have always expressed the total energy in terms of these two numbers, have then related R to θ through Eq. (4) [or more directly through Eq. (33)] and have then found the minimum energy contact angle θ. Our basic point is that including the details of the shape in the vicinity of the triple line is computationally expensive, difficult to check experimentally, and, at least in our devices, unnecessary to explain phenomena such as line tension and contact angle saturation.

It is possible to extend our framework to account for droplet deformation at the top electrode, and also for the shape of droplets between two planar electrodes, or between multiple electrodes of any shape. Instead of considering a truncated sphere whose shape is uniquely described by the two parameters R and θ, we consider a drop whose shape is described by a longer list of parameters $\mathbf{r}=(r_1,r_2,\ldots,r_n)$. For example, if the drop is rotationally symmetric, r_j could be a list of points that define the liquid/gas curve in the vertical plane. If the droplet is not symmetric, then the r_j's will define a discretized surface. To recast the analysis of Sec. II A, we find the energy E in terms of this shape vector $\mathbf{r}$ and physical parameters $\mathbf{p}$. This involves solving Maxwell's equations as a function of the shape $\mathbf{r}$. We then minimize $E(\mathbf{r},\mathbf{p})$ with respect to $\mathbf{r}$, subject to a constant volume constraint $\partial v(\mathbf{r})/\partial r = 0$, to find the minimum energy shape $\mathbf{r}^*$. Thus our semianalytic formulation is replaced by a purely numerical optimization. This formulation recovers droplet pinching at inserted electrodes, and it predicts the shapes of drops squashed between two planar electrodes. Detailed shape results for such cases will be presented in future publications.

e. *Numerical solution of the electrostatic PDEs plus scaling arguments:* For cases that involve electric fields, we have solved the Maxwell's PDEs that give rise to the electrostatic energy terms. Moreover, in each case we have first used a scaling argument to elucidate how the energy depends on parameters such as drop radius R, insulating solid height h, applied voltage V and material parameters like the conductivity and dielectric constants. Only after we have extracted all possible parametric dependencies, do we numerically solve Poisson's Eq. (28) for the θ shape dependence. It turns out that the scaling arguments (the liquid electric field goes as the voltage over radius, the liquid volume scales as radius cubed, the solid volume scales as radius squared times the height of the solid) can provide a tremendous amount of information. In fact, scaling arguments alone are sufficient to show when line tension terms do and do not exist. Scaling arguments reveal the underlying nondimensional numbers that capture the relative strength of the different physical effects, and scaling arguments can also be used to take full advantage of a limited set of numerical solutions. However, to predict the details of the θ shape changes we need to know how the electrical energy changes with contact angle and this requires numerical solutions of Eq. (28) for varying droplet shapes.

f. *Liquid resistance leads to contact angle saturation:* For our devices, we have found that including a small realistic amount of liquid resistance is sufficient to explain observed contact angle saturation data. Basically, the shape dependent resistance of the liquid drop leads to lower energy storage in the solid dielectric at small contact angles. Section IV C 5 provides a detailed analysis. Section V shows a comparison with experimental data.

ACKNOWLEDGMENTS

APPENDIX A: MATHEMATICAL DETAILS

Equations (8), (9), and (12) are all derived by partitioning the spherical drop into infinitesimally thin horizontal disks of varying radii and performing an integration over all the disks.

The double layer capacitive energy ratio result of Sec. IV A 4 is proved as follows. The Gouy–Chapman double layer theory outlined in Hiemenz and Rajagopalan[38] (Sec. 11.6) can be solved analytically for the potential in the double layer. Specifically, using normalized ($\hat{}$) variables

$$\hat{\phi}(\hat{y}) = 2\ln\left[\frac{1 - \dfrac{1-\exp(\hat{V}_l/2)}{1+\exp(\hat{V}_l/2)}e^{-\hat{y}}}{1 + \dfrac{1-\exp(\hat{V}_l/2)}{1+\exp(\hat{V}_l/2)}e^{-\hat{y}}}\right], \tag{A1}$$

where $\hat{\phi} = zF/RT\phi$ is the normalized potential in the double layer, $\hat{y} = y/\lambda_D$ is the normalized vertical distance away from the $y=0$ wall, $\lambda_D = \sqrt{\epsilon_l RT/2F^2 z^2 c_o}$ is the Deybe length scale, $\hat{\phi}(\hat{y}=0) = \hat{V}_l$ is the normalized potential at the wall, and z, F, R, T, c_o and ϵ_l are the charge number, Faraday constant, the gas constant, the far field ion concentration, and the dielectric constant of the liquid. Differentiating Eq. (A1) with respect to $\hat{y}$ gives the nondimensional electric field in the liquid $\hat{E}_l = -d\hat{\phi}/d\hat{y}$. Specifically, at the $\hat{y}=0$ wall

$$\hat{E}_l(\hat{y}=0) = -\frac{d\phi}{d\hat{y}}\Big|_{\hat{y}=0} = -2\sinh(\hat{V}_l/2). \tag{A2}$$

In Sec. IV A 4 we have a solid dielectric layer under the liquid ion layer. This layer has a dielectric constant ϵ_s and a voltage drop V_s. The total voltage drop across the liquid and the solid must equal the applied voltage $V = V_s + V_l$. Moreover, the electric field must satisfy the standard jump condition $\epsilon_s E_s = \epsilon_l E_l$, Feynman,[33] Vol. II, Chap. 10, where E_s is

the electric field in the solid at $y=0$. If the dielectric has height h_s, then by virtue of the fact that $E_s=V_s/h_s$ we recover (after normalization)

$$-2\sinh(\hat{V}_l/2)=\frac{\epsilon_s/\epsilon_l}{h_s/\lambda_D}\hat{V}_s. \tag{A3}$$

This can be inverted and then bounded from above

$$\hat{V}_l=2\sinh^{-1}\left(-\frac{\epsilon_s/\epsilon_l}{2h_s/\lambda_D}\hat{V}_s\right)\leqslant 2\sinh^{-1}\left(-\frac{\epsilon_s/\epsilon_l}{2h_s/\lambda_D}\hat{V}\right), \tag{A4}$$

where $\hat{V}$ is the voltage applied across the ionic double layer and the solid. The inequality follows from $\hat{V}_s=\hat{V}-\hat{V}_l\leqslant\hat{V}$. The energy of a single charge q located at height y above the wall is

$$u(y)=ez\frac{RT}{zF}\hat{\phi}(y/\lambda_d), \tag{A5}$$

where $e=1.6\times10^{-9}$ C is the elementary unit of charge. The charge per unit volume in the double layer is

$$n(y)=N_A[c_+(y)-c_-(y)]=N_Ac_o[\exp(-\hat{\phi})-\exp(\hat{\phi})]$$

$$=-2N_Ac_o\sinh\hat{\phi}(\hat{y}), \tag{A6}$$

where N_A is Avogadro's number. Multiplying Eqs. (A5) and (A6), and simplifying the dimensional coefficients, gives the net capacitive energy stored in the ionic double layer as

$$E_{\text{DL cap}}=\frac{1}{2}\frac{\epsilon_l}{\lambda_D}\left(\frac{RT}{zF}\right)^2\int_0^\infty -2\hat{\phi}(\hat{y})\sinh\hat{\phi}(\hat{y})d\hat{y}. \tag{A7}$$

The key point is that using $\hat{\phi}(\hat{y})$ from Eq. (A1) and the upper bound of Eq. (A4) it can be shown that the integral in Eq. (A7) is bounded by $(\epsilon_s\lambda_D\hat{V}/\epsilon_lh_s)^2$. Thus the capacitive energy stored in the ionic double layer is much smaller than the capacitive energy stored in the solid dielectric: $E_{\text{DL cap}}\leqslant(\epsilon_s\lambda_D/\epsilon_lh_s)E_{DEs}$. This is the result stated in Sec. IV A 4.

Numerical solutions of Maxwell's equations used in Figs. 4, 5, 7, 8, 9, 10, 11, 12, and 13 are carried out as follows. Poisson's equation are phrased in cylindrical coordinates with an assumed rotational symmetry about the z axis: $\nabla^2\phi(r,\alpha,z)=\partial^2\phi/\partial r^2+1/r\partial\phi/\partial r+\partial^2\phi/\partial z^2$. In all cases, we take $\nabla\phi_{\text{sides}}\cdot\hat{n}=0$ where $\hat{n}$ is the outward unit normal at the liquid/gas or liquid/solid boundary. This condition assumes that the dielectric constant of air ϵ_g is much smaller than that of the liquid ϵ_l or that of the solid ϵ_s. Boundary conditions for the remaining surface are outlined in the main text. The partial differential equations are discretized and solved using FEMLAB software (www.femlab-.com). Adaptive meshing is used because very high accuracy is required of the numerical solutions. Specifically, in Fig. 12 we need to accurately find the energy minima inside shallow wells. Even a 1% error in the numerical solution will lead to a significant lateral θ error in the energy minimum placement. The numerical solutions shown in Fig. 12, and thus also Fig. 13, are accurate to within 0.01%.

The solution scaling of Eq. (31) for the slightly resistive liquid atop a highly resistive dielectric solid is proved as follows. The proof proceeds by assuming that $\bar{\phi}$ is a valid

solution of the PDE and boundary conditions presented in Sec. IV C 2, and then showing that ϕ is also a valid solution. The original liquid solution $\bar{\phi}_l$ is multiplied by V and stretched by a factor of R in all three directions. A stretched and multiplied field still satisfies the necessary Laplace equation $\nabla^2\phi_l=0$ (within the liquid region $\rho=\rho_l$ is constant and may be moved outside the gradient operator), the voltage at the top of the drop goes from $\bar{\phi}_l(top)=\bar{V}=1$ to $\phi_l(top)=V$, the edges of the liquid solution are moved from $\bar{R}=1$ to R and $\nabla\phi_l\cdot\hat{n}$ remains zero at the liquid/gas interface. Likewise, the solid potential field $\bar{\phi}_s$ only has a z component (approximately), so if it is stretched by R in the x,y directions and by $h/\bar{h}$ in the z direction then it still satisfies $\nabla^2\phi_s=\partial^2\phi_s/\partial z^2=0$; the x,y scaling ensures that points just above and below the liquid/solid interface move together, and the multiplication of both $\bar{\phi}_l$ and $\bar{\phi}_s$ by V means that $\phi(x,y,z)$ remains continuous across the $z=0$ liquid/solid interface; finally $\phi(bottom)=0$ remains true. So the scaled field ϕ_l is a permissable solution in the liquid region, and ϕ_s is a permissable solution in the solid region; it only remains to show that the liquid/solid matching condition $\rho_s\partial\phi_l/\partial z=\rho_l\partial\phi_s/\partial z$ still holds. A stretching and magnifying of the potential fields creates the following scaled electric fields:

$$\mathbf{E}(x,y,z)$$

$$=\begin{cases}\nabla\phi_l(x,y,z)=\dfrac{V}{R}\bar{\nabla}\bar{\phi}_l^{\theta,\bar{A}}\left(\dfrac{x}{R},\dfrac{y}{R},\dfrac{z}{R}\right) & \text{in the liquid}\\[3mm]\nabla\phi_s(x,y,z)=\dfrac{\bar{h}V}{h}\bar{\nabla}\bar{\phi}_s^{\theta,\bar{A}}\left(\dfrac{x}{R},\dfrac{y}{R},\dfrac{\bar{h}z}{h}\right) & \text{in the solid.}\end{cases} \tag{A8}$$

Hence the liquid/solid electric field jump condition is now written

$$\rho_s\frac{\partial\phi_l}{\partial z}=\frac{\rho_sV}{R}\frac{\partial\bar{\phi}_l}{\partial\bar{z}}=\frac{\rho_l\bar{h}V}{h}\frac{\partial\bar{\phi}_s}{\partial\bar{z}}=\rho_l\frac{\partial\phi_s}{\partial z}. \tag{A9}$$

But $\bar{\rho}_s\partial\bar{\phi}_l/\partial\bar{z}=\bar{\rho}_l\partial\bar{\phi}_s/\partial\bar{z}$ with $\bar{\rho}_s/\bar{\rho}_l=\bar{A}$, thus $\partial\bar{\phi}_s/\partial\bar{z}=\bar{A}\partial\bar{\phi}_l/\partial\bar{z}$, substituting this into equation (A9) gives, after rearrangement and cancelation of the $\partial\bar{\phi}_l/\partial\bar{z}$ term, $\bar{A}=\bar{\rho}_s/\bar{\rho}_l=\rho_sh/\bar{h}/\rho_lR$. So the last necessary boundary condition is still satisfied when $\bar{A}$ is chosen in this way.

[1] B. Berge, Acad. Sci. Paris C.R. **317**, 157 (1993).
[2] M. Vallet, B. Berge, and L. Vovelle, Polymer **37**, 2465 (1996).
[3] C. Kim and J. Lee, *Proceedings Conference of IEEE Micro Electro Mechanical Systems Workshop*, Heidelberg, Germany, 1998, pp. 538–543.
[4] V. Peykov, A. Quinn, and J. Ralston, Colloid Polym. Sci. **278**, 789 (2000).
[5] H. Verheijen and W. Prins, Langmuir **15**, 6616 (1999).
[6] M. Vallet, M. Vallade, and B. Berge, Eur. Phys. J. B **11**, 583 (1999).
[7] T. Blake, A. Clarke, and E. Stattersfield, Langmuir **16**, 2928 (2000).
[8] M. Pollack, R. Fair, and A. Shenderov, Appl. Phys. Lett. **77**, 1725 (2000).
[9] E. Seyrat and R. Hayes, J. Appl. Phys. **90**, 1383 (2001).
[10] J. Lee, H. Moon, J. Fowler, T. Shoellhammer, and C. Kim, Sens. Actuators A **95**, 269 (2002).
[11] G. Lippmann, Ann. Chim. Phys. **5**, 494 (1875).
[12] R. Probstein, *Physicochemical Hydrodynamics, An Introduction* (Wiley, New York, 1994).

[13] R. Hansen and T. Toong, J. Colloid Interface Sci. **37**, 196 (1971).

[14] E. Dussan and S. Davis, J. Fluid Mech. **65**, 71 (1974).

[15] E. Dussan V, Annu. Rev. Fluid Mech. **11**, 371 (1979).

[16] P. deGennes, Rev. Mod. Phys. **57**, 827 (1985).

[17] R. Cox, J. Fluid Mech. **168**, 169 (1986).

[18] M. Smith, J. Fluid Mech. **294**, 209 (1999).

[19] S. Benintendi and M. Smith, Phys. Fluids **11**, 982 (1999).

[20] C. Decamps and J. De Coninck, Langmuir **16**, 10150 (2000).

[21] A. Marmur, J. Imaging Sci. Technol. **44**, 406 (2000).

[22] Y. Gu, Colloids Surf., A **181**, 215 (2001).

[23] A. Torkkeli, J. Saarilahti, A. Haara, H. Harma, T. Soukka, and P. Tolonen, *Proceedings Conference of MEMS 2001. 14th IEEE International Conference on Micro Electro Mechanical Systems*, 2001.

[24] H. Moon, S. Cho, R. Garrell, and C. Kim, J. Appl. Phys. **92**, 4080 (2002).

[25] H. Ren, R. Fair, M. Pollack, and E. Shaughnessy, Sens. Actuators B **87**, 4346 (2002).

[26] R. Digilov, Langmuir **16**, 6719 (2000).

[27] W. van der Vegt, W. Norde, H. van der Mel, and H. Busscher, J. Colloid Interface Sci. **179**, 57 (1996).

[28] M. Butkus and D. Grasso, J. Colloid Interface Sci. **200**, 172 (1998).

[29] J. Lyklema, *Fundamentals of Colloid and Interfaces Science, Volume II: Solid Liquid Interfaces* (Academic, London, 1995).

[30] T. Chou, Phys. Rev. Lett. **87**, 106101 (2001).

[31] R. Zimmermann, S. Dukhin, and C. Werner, J. Phys. Chem. B **105**, 8544 (2001).

[32] L. Koopal and M. Avena, Colloids Surf., A **192**, 93 (2001).

[33] R. Feynman, R. Leighton, and M. Sands, *The Feynman Lectures on Physics* (Addison–Wesley, Reading, MA, 1964).

[34] K. Brakke, Exp. Math. **1**, 141 (1992).

[35] S. Cho, S. Fan, H. Moon, and C. Kim, *Proceedings of IEEE International Conference on Micro Electro Mechanical Systems, Las Vegas, NV*, 2002, pp. 32–52.

[36] A. Beskok, *Proceedings Conference of AIAA 39th Aerospace Sciences Meeting and Exhibit*, 2001.

[37] P. deGennes, *Soft Interfaces, The 1994 DIRAC Memorial Lecture* (Cambridge University Press, Cambridge, 1994).

[38] P. Hiemenz and R. Rajagopalan, *Principles of Colloid and Surface Chemistry* (Dekker, New York, 1997).

[39] D. Lide, *CRC Handbook of Chemistry and Physics*, 82nd ed. (CRC, Boca Raton, 2002). 82nd ed.